Convolutional neural network for predicting crack pattern and stress-crack width curve of air-void structure in 3D printed concrete

Chang, Ze; Wan, Zhi; Xu, Yading; Schlangen, Erik; Šavija, Branko

DOI
10.1016/j.engfracmech.2022.108624

Publication date
2022

Document Version
Final published version

Published in
Engineering Fracture Mechanics

Engineering Fracture Mechanics 271 (2022) 108624

Contents lists available at ScienceDirect

Engineering Fracture Mechanics

journal homepage: www.elsevier.com/locate/engfracmech

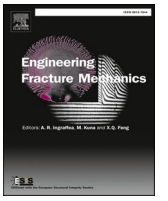

Convolutional neural network for predicting crack pattern and stress-crack width curve of air-void structure in 3D printed concrete

Ze Chang, Zhi Wan *, Yading Xu, Erik Schlangen, Branko Šavija

Microlab, Faculty of Civil Engineering and Geosciences, Delft University of Technology, Delft, the Netherlands

ARTICLE INFO

Keywords:
Air-void structure
Crack pattern
Convolutional neural network
Transfer learning

ABSTRACT

Extrusion-based 3D concrete printing (3DCP) results in deposited materials with complex microstructures that have high porosity and distinct anisotropy. Due to the material heterogeneity and rapid growth of cracks, fracture analysis in these air-void structures is often complex, resulting in a high computational cost. This study proposes a convolutional neural network (CNN)-based methodology for fracture analysis using air-void structures as input. More specifically, the lattice fracture model is used to build a dataset that comprises input air-void structures as well as output fracture information, including the crack patterns and crack-width curves. To establish the relationship between crack morphology and associated microstructures, a U-net convolutional neural network is first presented. With the obtained crack pattern as input, the principal component analysis (PCA) and CNN are then integrated to predict the stress-crack width curves. The predicted results from the CNN model demonstrate a quantitative agreement with lattice numerical analyses, with 0.85 Intersection over Union for crack patterns prediction and 0.75 R^2 for the stress-crack width curves prediction. This indicates that CNN models can be used as an alternative to traditional numerical analysis. The feature maps during the convolutional or deconvolutional process are given to explain why the proposed CNN models perform well on fracture analysis of the air-void system. Moreover, the model generalization is discussed using transfer learning with fine-tuning to show the model potential on microstructures expressing varied pore information. In the end, the microstructures cropped from XCT are created to explore the further application of CNN models on fracture analysis of 3D printed materials.

1. Introduction

3D concrete printing (3DCP) is considered an ongoing revolution to modernize construction. This emerging fabrication technique can produce complex structural components while reducing the use of formworks. Such an additive manufacturing method enlarges the possibilities in producing elegant, labour-saving building components with minimal material use, and speeds up the production

Abbreviations: 3DCP, 3D concrete printing; LSTM, Long short-term memory; RNN, Recurrent neural network; PCA, principal component analysis; CNN, convolutional neural network; FEM, finite element method; ML, machine learning; IoU, Intersection of Union; CEV, cumulative explained variance; MSE, Mean Squared Error; ReLU, Rectified Linear Unit; GPA, Global average activation function; TL, transfer learning.

* Corresponding author.
E-mail addresses: Z.Chang-1@tudelft.nl (Z. Chang), Z.Wan-1@tudelft.nl (Z. Wan), Y.Xu-5@tudelft.nl (Y. Xu), Erik.Schlangen@tudelft.nl (E. Schlangen), B.Savija@tudelft.nl (B. Šavija).

https://doi.org/10.1016/j.engfracmech.2022.108624
Received 29 March 2022; Received in revised form 1 June 2022; Accepted 13 June 2022
Available online 15 June 2022

process considerably [1,2].

A price is, however, to be paid for these advantages. In contrast to the conventional construction methods, a weak zone is created at a layer-by-layer interface due to the extrusion process, resulting in material anisotropy; this significantly affects the mechanical behaviours of 3D printed samples, such as tensile and flexural strength [3,4]. Recent experiments study the impact of printing parameters and curing conditions on the interlayer bond strength of 3D printed samples [4–8]. These findings suggest that the interlayer bonding (i.e., the interparticle friction and cohesion between adjacent layers) is determined by the air void distribution, the connectivity of the capillary pore structure and the mechanical strength of the cementitious matrix at the interface [3,9,10]. A deeper insight into the air-void effect on interlayer bonding strength is obtained from numerical analyses, from which the impact of air-void size and distribution on material properties and fracture behaviour is quantitatively studied [4,5,7,11,12]. Although these simulations provide an in-depth explanation for the fracture mechanism of air-void systems, the complexities caused by the heterogeneity still put burdens on computational efficiency. Most numerical models used are computationally expensive since a fine mesh is required to accommodate stress concentration near the crack tip. In addition, high-quality meshes and complicated re-meshing are required in the finite element method (FEM) to handle non-continuum interface due to crack generation and growth [13–17].

Therefore, a powerful and highly efficient tool is required to handle these challenges. A machine learning (ML) approach can accurately capture the importance of input features to make intelligent decisions. Recently, this advanced technology has been applied to mechanical analysis [18–22], structure optimization [23,24], mix design [25–27], and health monitoring [28,29]. Such machine learning-based models do not require significant human intervention and knowledge of fracture mechanics, while they can efficiently build the relationship that involves the features extracted from the inputs and outputs.

The convolutional neural network (CNN) is a type of artificial neural network and it can be regarded as a standout image identification method among ML algorithms. In light of image processing, traditional neural networks must import the images in the form of reduced-resolution pieces. In contrast, the CNN has a system like a multilayer perceptron which avoids the piecemeal image processing issue. This removal of limitations and increase in efficiency for image processing ensure a far more effective system for image analysis. Previous studies show that the CNN has a superior performance in structural health monitoring tasks such as identification and segmentation of concrete cracks [30,31]. In addition, CNN has also been adopted for discriminative refocusing of microstructural images [20,32] and phase-detection [33], which verify the application of CNN in material science. Recently, several researchers explored the application of CNN in predicting mechanical behaviours of heterogeneous materials [20,34,35]. Yang et al. [20] combined the CNN and principal component analysis (PCA) to predict the stress–strain curves of binary composites over the entire failure process. A mean absolute error below 10% can be derived for model performance evaluation. Similarly, Kim et al. [35] adopted CNN to predict and validate the transverse mechanical properties of complex, unidirectional composites considering the interfacial demolding. These successful cases confirmed that the CNN model can efficiently clarify the relation between the microstructure and material properties. In the context of fracture analysis, several machine learning methods have been proposed to conduct fracture analysis in different materials [36–40]. They can be divided into two categories based on the expected outcome, i.e., the fracture parameters and crack pattern prediction. The ability to predict the crack pattern allows for a comprehensive understanding of fracture behaviour. Several noteworthy studies can be found in the literature [36,37,40,41]. Hsu et al. [36] combined the CNN and Long short-term memory (LSTM) to predict the fracture patterns in crystalline solids. The predicted results show excellent agreement in terms of computed fracture pattern. Similarly, Elapolu et al. [37] adopted a machine learning model to predict the brittle fracture of polycrystalline graphene subjected to tensile loading. The predicted crack growth agrees well with the molecular dynamics simulation. Wang et al. [40] adjusted a deep learning model, StressNet, to simulate the entire sequence of internal stress distribution with the crack propagation and initial stress as input. A typical feature of these machine learning techniques is to combine CNN and Recurrent neural network (RNN). In particular, the CNN model aims to extract features from the input images, and RNN can learn the connectivity of elements in a sequence. Through this method, the crack pattern is represented through the pixel value in the output image that is usually transferred or reshape from a vector after fully connected layer. Therefore, the entire crack information is represented by a series slice of image and each slice is computed through one round learning process. In this work, a U-net model is employed to directly predict the crack morphology image based on the material microstructure and the air-void system. The entire crack information is present through a matrix after one cycle of learning. Through this improved method, the fracture behaviour of the 3D printed materials will be studied instantaneously for the first time, avoiding the computational costs associated with traditional numerical analysis.

In this study, two databases that contain different air-void digital images were first created based on the air-void distribution in 3DCP. The lattice fracture model was then utilized to get the stress-crack width curves and crack patterns for input microstructures subjected to uniaxial tension. A U-net CNN was proposed to establish the relationship between the crack pattern and corresponding binary image. Based on the microstructural cracks, a CNN model combined with PCA was then trained for stress-crack width curve prediction. The model performance was evaluated by a customized loss function, R^2 and Intersection over Union (IoU). Finally, a discussion about model generalization is given using the transfer learning with fine-tuning.

This work is structured as follows. Section 2 provides the physical theory of the lattice fracture model and the procedures of database generation. Then, an introduction about the model architecture and customized parameters is given in Section 3. Model performance is presented in Section 4, together with the generalization capability of learning algorithms.

2. Lattice fracture model

3D concrete printing produces air-void structures with obvious anisotropic behaviour in terms of uniaxial tensile strength [4,7]. This can be partly attributed to the air-void distribution due to the layer-by-layer technique. To study the impact of air-void distribution on mechanical and fracture behaviour, the lattice fracture model is adopted to do the computational uniaxial tensile tests of air-

void structures. Numerical modelling has been utilized since the early 90′s for fracture analysis in composite materials such as concrete and mortar [17,42,43]. Recently, numerical modelling has been extended to model the mass transfer [44] and 3D concrete printing [45]. In general, the lattice model comprises two advantages: (1) In contrast with FEM-based methods, the lattice model can avoid singularity-related issues based on discontinuous formulation; (2) Material heterogeneity is easily implemented in lattice models.

2.1. Basic principles of the lattice model

In the lattice model, the continuum object is schematized as a network of Timoshenko beams that can transfer normal forces, shear forces and bending moments. The model is subjected to external loading and boundary conditions. Then, a series of linear elastic analyses are conducted by computing the comparative stress of each element using the following equation.

$$\sigma = \alpha_{\mathrm{N}}\frac{F}{A}+\alpha_{\mathrm{M}}\frac{\left(|M_i|,|M_j|\right)_{\max}}{W} \tag{1}$$

in which A is the cross-sectional area and W refers to the bending moment resistance, both are identical for all elements; i and j are two adjacent lattice nodes of each element in the local coordinate system. N and M represent normal force and bending moment which act on lattice elements. Also, σ is the comparative element stress after each step analysis. Two coefficients, namely, α_{N} and α_{M}, govern the impact of normal force and bending moment on material failure. Based on our previous research [17], their values are adopted as 1.0 and 0.05.

During the numerical analyses, the prescribed displacement is applied into the system until exactly one lattice element reaches the material tensile strength. This element is then removed from the lattice model, representing a small crack during loading process. The model is then relaxed and this loading procedure is repeated with the updated structural stiffness until the lattice mesh breaks into two parts.

2.2. Air-void structure generation

To create a database that mimics an air-void systems in 3DCP, a fundamental understanding of air-void characterization of a 3D printed sample is required. Fig. 1 describes the air-void distribution along with the height of 3D printed sample in micro-scale (i.e., the cumulative air-void content of each row in the binary image), and detailed information about this sample can be found from our previous research [5]. It can be illustrated that the printed specimen exhibits a much higher local porosity at the interlayer zone in contrast to the printed layers zones.

In view of the air-void characterization of 3D printed sample, a microstructure generation algorithm is developed through a MATLAB-based code, which enables the creation of a two-phase material structure (i.e., air-void and solid phase). Considering the computational capacity, the binary image is set to 32 by 32 pixels, in which the maximum number of pores is 6. According to the air-void distribution in 3D printed sample, the air-voids are generated along with image height using normal distribution function (mean value is 16 and the standard deviation is 8). In this way, an air-void has the largest probability to be placed on the interlayer zone, as shown in Fig. 2 (a). Here, two distinct datasets with different characteristics of air-void information are built. Group 1, which contains microstructures with the three air-voids of 3.5 mm diameter, is created for model training and testing, as shown in Fig. 2 (b). On the other hand, group 2 with quite different features in terms of size and number of air voids is adopted to discuss model generalization. The typical microstructures from dataset 2 can be found in Fig. 2 (c).

These pixel-based material structures are then mapped onto a lattice mesh to implement the material heterogeneity. Different local mechanical properties are assigned to lattice elements based on node positions. Fig. 3 describes the detailed procedures as follows: (a) The continuum object is divided into a grid of cells. (b) A sub-cell is generated in the centre of each cell, and a lattice node is placed in the middle of this sub-cell. (c) Timoshenko beams are utilized to connect the adjacent lattice nodes (horizontal and vertical).

2.3. Computational uniaxial tensile test

A typical example of lattice mesh derived from the binary image is shown in Fig. 2 (a). The fracture analyses of air-void systems are then performed subject to uniaxial loading, with the bottom fixed and a prescribed displacement applied on the top side, as shown in Fig. 4 (a). Local mechanical properties of the matrix, including the elastic modulus E, shear modulus G, and tensile strength f_{t} are

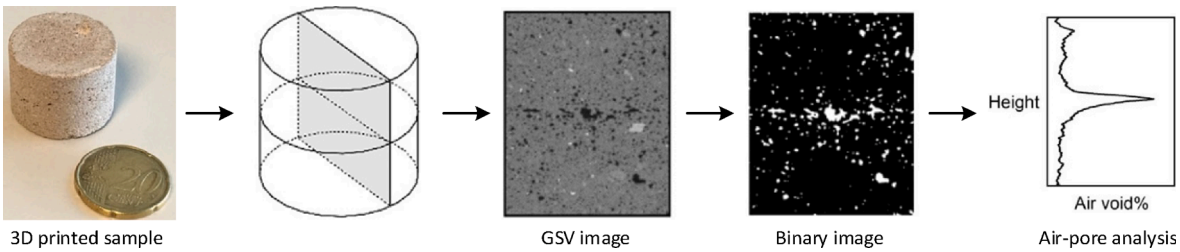

Fig. 1. Illustration of microstructure and air-void analysis of 3D printed sample [5]

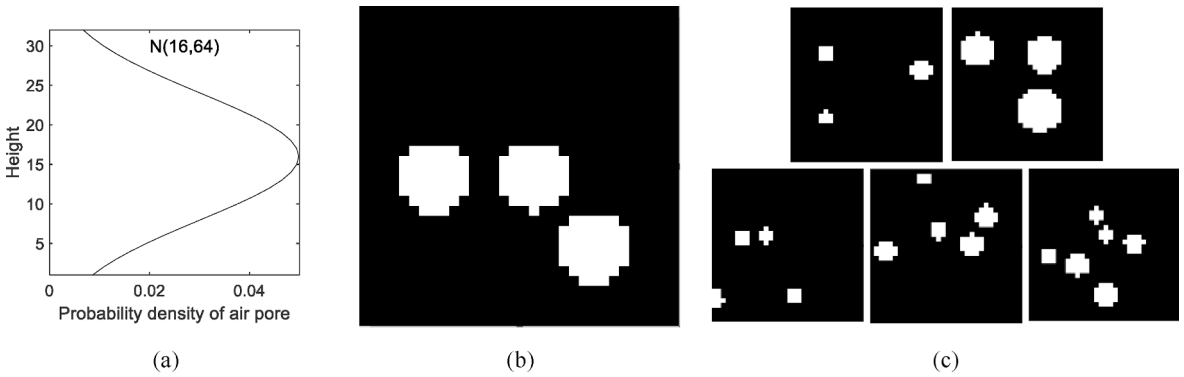

Fig. 2. A schematic overview of generalized microstructures (a) air-void distribution; (b) microstructure from dataset 1; (c) typical microstructures from dataset 2.

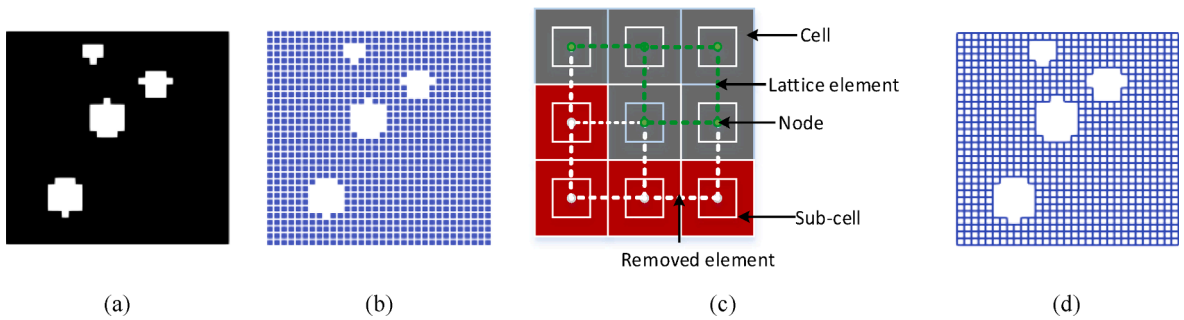

Fig. 3. Illustration of lattice model generation: (a) digital material structure; (b) lattice nodes in mesh system; (c) the overlay procedure for 2D lattice mesh (red-air voids, grey: solid phases); (d) the meshed 2D lattice network;

derived from previous research [7]. In each analysis step, the lattice beam with the highest ratio of stress and strength is marked and removed from the mesh system to mimic a small crack, as shown in Fig. 4 (b). Two adjacent lattice nodes connected by a broken element represent a crack pixel, thus, the crack pattern can be derived for a given binary image (as shown in Fig. 4 (c)). From the analysis, a stress-displacement response at each step can be derived. Since the lattice model adopts the sequentially-linear analysis method, snap-back behaviour can be observed in the simulated response, as shown in Fig. 4 (d). For more detailed information about the crack behaviour, it is possible to eliminate the elastic deformation from the stress-displacement curve to get the stress-crack width diagram, as shown in Fig. 4 (e). This relationship is then collected as a stress vector, which represents the stress-crack width curve via an array of stress values which are evaluated at 101 points with a 0.1 micro interval, as shown in Fig. 4 (f). This stress vector is adopted as the target in CNN model for stress-crack width curve prediction.

3. Methodology

This study proposes two CNN models to replace the conventional FEM models for mechanical and fracture analyses of air-void systems. The goal of the first model is to reproduce the crack pattern based on the microstructure while the second one aims to predict the stress-crack width curve with the crack pattern as input. The microscale lattice model for the uniaxial tensile test is adopted to create a dataset. Here, the database from group 1 is employed to train and validate the CNN models. The dataset from group 2 is adopted for discussion of model.

3.1. U-Net model for crack pattern prediction

This section proposes a U-net CNN model to clarify the relationship between the crack pattern and microstructure consisting of air-voids and solid phases. The Intersection over Union (IoU) is employed to evaluate model performance (see Eq. (2)).

3.1.1. IoU identification

The inherent problem of crack prediction is a classification problem, in which each pixel needs to be labelled as either a crack or a solid phase. This kind of classification problem generally adopts the metrics to assess model accuracy, in which the model performance is evaluated using the ratio between the correct predictive quantity and the total number of predictions. This kind of binary/multi classification makes computing accuracy straightforward. However, it is not suitable for crack prediction as the small amount of crack

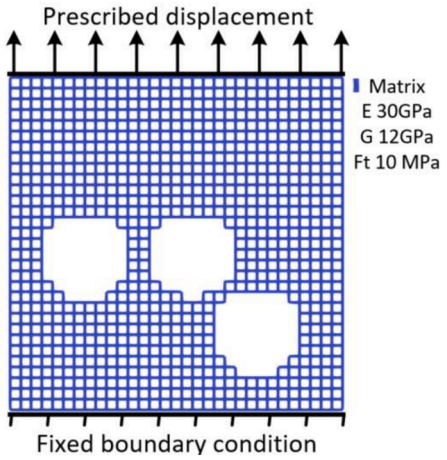

(a)

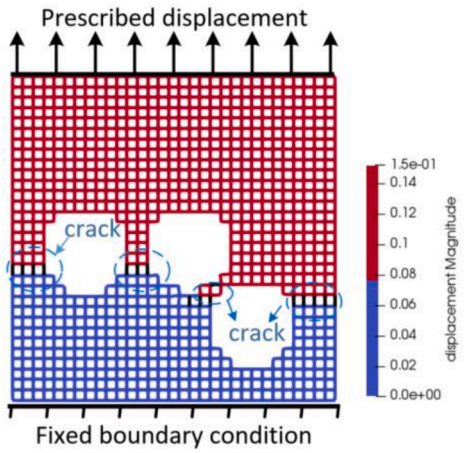

(b)

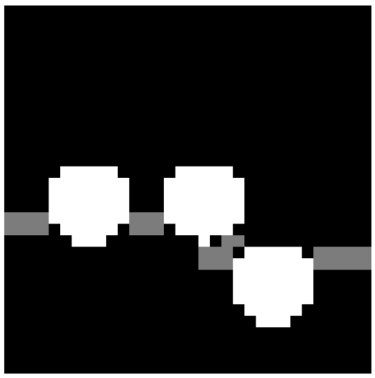

(c)

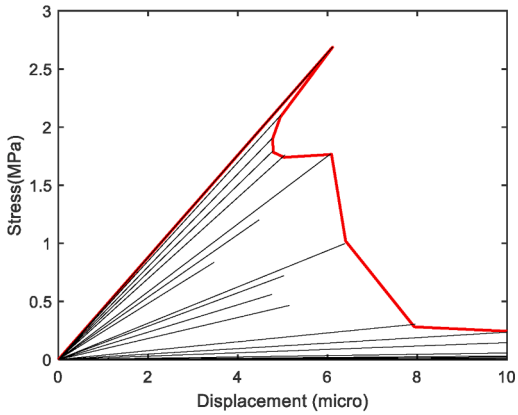

(d)

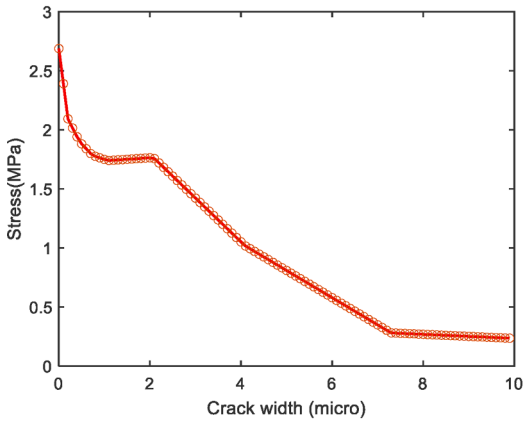

(e)

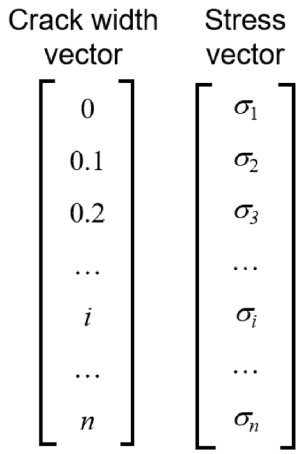

(f)

Fig. 4. (a) The lattice mesh with boundary condition (b) Simulated crack pattern using the lattice model (black: crack) (c) Output crack pattern in CCN (Gray: crack; white: pore; black: solid-matrix) (d) The simulated stress–strain curve in lattice model (e) the simulated stress-crack width diagram (f) model target for stress-crack width prediction.

in this research may produce 'fake' high accuracy using binary classification. The Intersection over Union (IoU) is a standard index for semantic segmentation problems [46]. This study adopts it to evaluate model performance, which is the overlap ratio of the predicted crack zone and the numerical results derived from the lattice fracture model. The calculation method and relevant cases can be found in Eq. (2) and Fig. 5. When comparing the predicted crack pattern (two phases: solid and crack) with the microstructure only including the solid phase, the computed IoU is around 0.47 which suggests a large space for model training.

$$\text{IoU} = \frac{\text{Overlap}}{\text{Union}} \tag{2}$$

3.1.2. U-net CNN model design

This study aims to predict the crack pattern image with the same dimensional information of input microstructure, it requires a network to describe the rough feature map and then fills in details. U-Net is a CNN model in symmetric U shape that was developed for biomedical image segmentation at the Computer Science Department of the University of Freiburg [47]. The model reproduces the image information including segmentation or localization with the same dimensions as the input image. In this study, the model framework is inherited from previously published research work [47], with the majority of hyperparameters remaining the same. The hyperparameter analyses are therefore not extensively performed herein. In detail, U-net includes two blocks, as shown in Fig. 6. The first path is the down-sampling block (also named the encoder), which was composed of a sequence of convolutional layers using the Rectified Linear Unit (ReLU) activation function and max-pooling layers. The goal of this block is to extract and capture the context in the input image. The convolution and pooling processes generate smaller feature maps than the input binary image. Therefore, an up-sampling path or a decoder is required to expand the feature maps, and it enables precise localization through transposed convolutions. This up-sampling block that contains a series of deconvolutional and convolutional layers is combined with the concatenation process with relevant feature maps from the down-sampling process. These feature maps from the down-sampling process carry lots of spatial information and are then connected to the feature maps in the decoder path. Many feature channels in the expansion path are obtained, and they allow the network to pass the context information to higher resolution layers.

The decoder process is approximately symmetric to the encoder path in the U-net framework. Detailed information about the model architecture can be found in Fig. 6. A binary image depicting a specific microstructure is fed into the U-net model as input. Then, this image is processed through two convolutional layers and activated by the ReLU function. Subsequently, the stacked feature maps derived from the convolutional layers are processed via Conv block 2 to Con block 5, each of which contains one max-pooling layer and two convolutional layers followed by ReLU activation functions. The feature map from the encoder's last logit is processed by a single up convolutional layer during the up-sampling process. This result is then concatenated with the feature map from the encoder process with the same spatial resolution. After that, two convolutional layers and one deconvolutional layer are utilized to analyze and form a new feature map. This process is repeated three times until the size of the feature map is equal to the input image. The final computed feature map is processed by two convolution processes, and the crack pattern can eventually be obtained. For model training and validation, the total dataset is 193,989. This model uses a split train-test dataset ratio of around 95:5, in which the test set size is roughly 9,000 and enough for model validation. The batch size for all sets is set to 64 and the learning rate is 0.0003 using Adam optimizer.

3.1.2.1. Deconvolutional layer. In the U-net CNN model, the down-sampling block convolves the input image to a rough image with low resolution and high-level description. Considering the predicted crack patterns are in the same dimensional information as input microstructures, it requires the network to describe the rough feature map and then fill in the details. The deconvolutional layers provide the solution to extract information of each point from the input feature map to reproduce a larger one. The deconvolution operation is carried out by sliding a filter (i.e., deconvolutional kernel) over the rough image step by step Fig. 7. During every sliding operation, the coved area by the filter is called the receptive field, which is composed of a matrix of greyscale values. Like the convolution process, the dot product computed by the filter and matrix is taken as the local feature of the input image for subsequent layers.

3.2. CNN model for stress-crack width curve prediction

3.2.1. Principal component analysis (PCA) for dimensionality reduction

Besides the crack pattern, stress-crack width curve is another descriptor that reflects the impact of microstructure and crack growth on mechanical behaviour. Considering that the stress-crack width curve is represented by a vector of stress values comprising 101

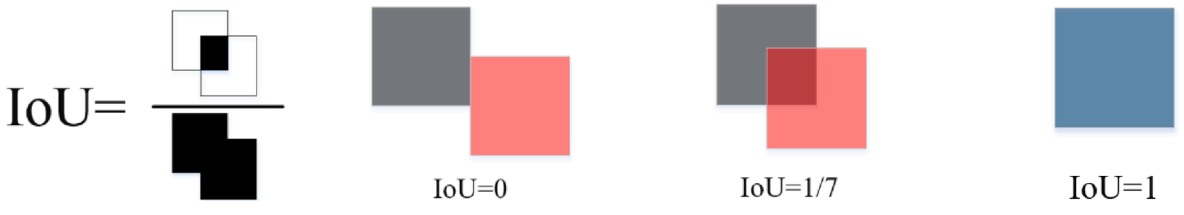

Fig. 5. A schematic diagram of an IoU computation and typical examples.

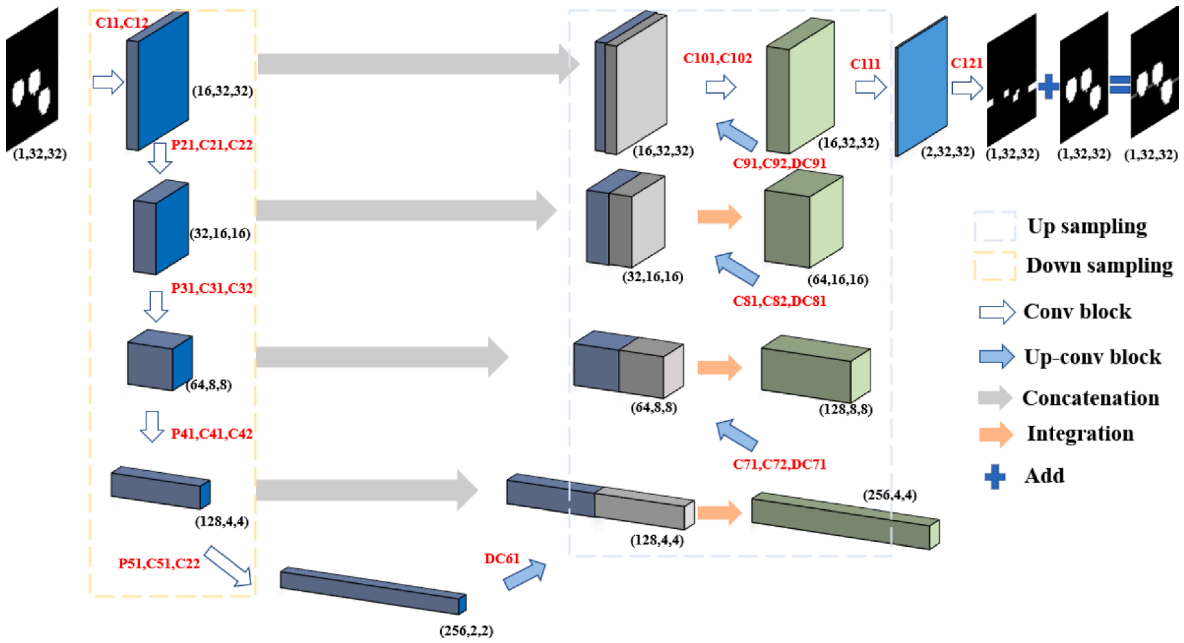

Fig. 6. U-Net neural network (C#: Convolutional layer; P# Max pooling layer; DC#: Deconvolutional layer; LR# activation layer).

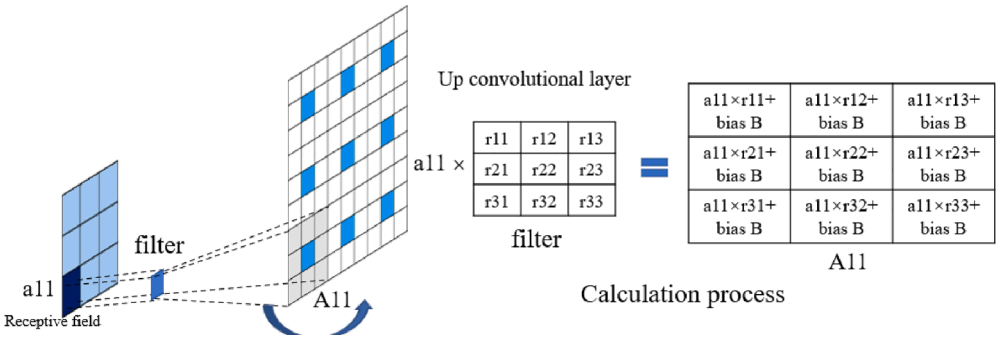

Fig. 7. Illustration of deconvolutional layer.

displacement points with a 0.1 micro interval, this high dimensionality of the dataset significantly increases the difficulty of the prediction model. The principal component analysis (PCA) is used to analyze the relationship among the inputs and reduce the dimensionality of the stress vector, thereby decreasing computational cost.

PCA is a multivariate technique and its fundamental principle is to reduce the dimensionality while keeping most features of the original dataset through limited inter-correlated quantitative dependent variables. During the dimensionality reduction process, the size of the original data is compressed by retaining important features. A simplified description is proposed to represent a similar pattern of observation using several dependent parameters, which are derived after handling the heterogeneous sets of variables. These new variables called principal components keep the linear combination of the original variables, which are eigenvectors of the covariance matrix of the original data. The first principal component has the largest possible variance to describe the characteristics of the data table. The other components are computed under the constraint of being orthogonal to each other.

In this study, the stress-crack width curve of the dataset is expressed as X matrix with $n \times m$ dimensionality, in which each row represents an individual dataset and each column provides a stress value at a given strain interval. Considering that the strain vector adopts the same values and lengths across all datasets, only the stress vector is passed to the X matrix for dimensionality reduction through PCA. The matrix $\overline{X}$ with column mean is calculated by centralizing the matrix X based on the mean of each column (i.e., μ) [20].

$$\overline{X} = X - \mu \tag{3}$$

The principal component transformation is then computed through the singular value decomposition (SVD), shown in Eq. (4).

$$\overline{X} = U\Sigma W^T \tag{4}$$

where U is an $n \times n$ matrix in which the columns are orthogonal unit vectors; Σ is an $n \times m$ diagonal matrix storing positive singular values (i.e., square roots of the principal component variances); W^T includes the principal components in the order of decreased variance explained λ which are computed based on singular value decomposition of the covariance matrix. Using this technique, each dataset can be transformed by projecting the stress vector into a new set of coordinates with lower-dimensional latent space. The cumulative explained variance (CEV) represents the summation of eigenvalues normalized by the sum of eigenvalues with the number of r, shown in Eq. (5).

$$CEV(r) = \sum_{i=1}^{r} \lambda_i / \sum_{j=1}^{200} \lambda_j \tag{5}$$

In this study, the open-source Python scikit-learn package [48] is employed to implement PCA for dimensionality reduction. After dimensionality reduction, the proposed CNN model can learn more efficiently under a lower-dimensional space. Therefore, a higher accuracy with the same training data can be obtained using the identical CNN architecture.

3.2.2. Model evolution

In PCA, each eigenvalue allows for the explained variance (i.e., proportion of variance accounted for) of the relevant principal component basis-vector. To denote their different weights in the CNN model towards stress-crack width curve prediction, a customized loss function (adjusted Mean Squared Error (MSE)) and an evaluation index (adjusted coefficient of Determination (R^2)) are constructed. In the customized loss function (i.e., adjusted MSE) and model evaluation coefficient (i.e., adjusted R^2), the principal components with higher explained variance are weighted heavier than those with low explained variance, as shown in Eq. (6) [20].

$$\begin{aligned} AdjustedMSE &= \sum_{i=1}^{n} \sum_{j=1}^{r} \frac{\lambda_i}{\sum_{k=1}^{24} \lambda_k} \left(y_{i,j} - y_j^*\right)^2 \\ Adjusted R^2 &= \sum_{j=1}^{r} \frac{\lambda_i}{\sum_{k=1}^{24} \lambda_k} \left[1 - \frac{\sum_{i=1}^{n} \left(y_{i,j} - y_{i,j}^*\right)^2}{\sum_{i=1}^{n} \left(y_{i,j} - \overline{y}_j^*\right)^2}\right] \end{aligned} \tag{6}$$

where the $y_{i,j}$ and $y_{i,j}^*$refers to the actual and predicted values of i-th sample in j-th feature, and $\overline{y}_j$ is the mean value of calculated stress on j-th column. Using the adjusted MSE and R^2, each component in the stress vector has its specific component coordinate to interact with our CNN about their different importance for model training and model performance evaluation.

3.2.3. CNN implementation and training

In this section, based on the previous research work [20], a CNN model is utilized to predict the reduced-dimensional stress-crack width curve using the microstructural crack as input. The number of the dataset is 132,883. This model uses a split train-test dataset ratio of 94:6, in which the test set size is roughly 8,000 and enough for model validation. The batch size for all sets is set to 64. A shuffling strategy is adopted to enable the CNN model to efficiently learn and extract the features of microstructures without the impact of sequence. This CNN model is built on the torch backends. The Adam optimizer with a learning rate of 0.0001 is employed to update the weights of trainable parameters during backpropagation.

In this study, the fully convolutional neural network with 4 Conv blocks is adopted, which is shown in Fig. 8. There are 6 kinds of

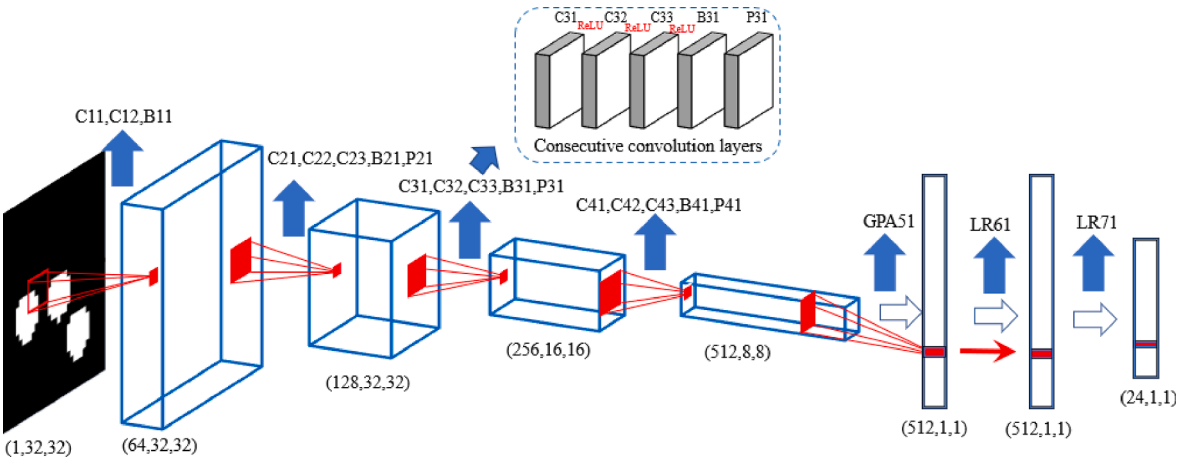

Fig. 8. CNN architecture (C#: Convolutional layer; B#: Batch normalization layer; P# Max pooling layer; GPA: Global average activation function; LR# activation layer).

layers in this network, namely the convolutional layer, ReLU, Batch Normalization layer, max-pooling layer, global pooling layer, and linear activation layer. Fig. 8 shows that the input layer receives representative microstructures in binary images. These images are then passed into the first Conv block including two convolutional layers with ReLU activation function followed by Batch Normalization. Subsequently, these stacked feature maps produced by the first Conv block are analyzed via Conv block 2 to Con block 4. These 3 blocks share the same architecture, i.e., three convolutional layers using a ReLU activation followed by Batch normalization and max-pooling layer. In the end, the stacked feature maps are flattened using a global max-pooling layer to derive a vector with the size of 512. A liner activation layer is adopted to transfer this vector into 24 scalars, which is the decreased dimensionality number after PCA.

3.2.3.1. Consecutive convolutional layer. In the CNN model, the convolutional layer is what makes the CNN model stand out from artificial neural network when it comes to image identification. It can be seen from Fig. 9 that the convolution operation is essentially a step-by-step sliding process of a filter (i.e., kernel) over the whole binary image. The filter is a matrix consisting of a series of trainable parameters with a size smaller than the input image. The area corresponding to the convolutional filter is defined as the receptive field, which is a matrix of greyscale value and whose size is equal to that of the filter. In the convolutional layer, the dot product computed by the filter matrix and receptive filed matrix is derived. The local features of the input image are then extracted to form new features, which are activated using a non-linear function such as ReLU. The output feature map is then transferred to the subsequent convolutional layer. During the convolution operation, the filter plays a dominant role in the formation of a feature map. A larger filter produces a larger receptive field including more information at each step. However, it also puts a burden on the computational capacity. Here, considering the computer memory and processing time, the filter with the size of 3*3 and stride of 1 is employed for feature extraction.

3.2.3.2. Pooling layer. Besides convolutional layers, the pooling layer is another module to distinguish CNN from other ML networks. After the convolution operation, the derived feature map usually has largely augmented dimensions, which raise a problem of computational inefficiency. In the view of this case, the pooling layer is incorporated into the CNN model to decrease the dimension of the feature map and retain the important information extracted from the convolutional layer. Fig. 10 describes how the pooling layer works in CNN. Like the convolution process, a pooling filter is incorporated into the pooling layer to slide over the feature maps. The part of feature maps covered by the pooling filter is the pooling field, in which the max or average value is computed to form the downscaled feature map. In this study, the max-pooling layer with the filter size of 2*2 and stride of 2 is utilized to decrease the dimensionality of the feature map. After all convolution processes, a global average pooling layer is employed to calculate the average feature map in each channel and generate a 1D vector for the next dense layer, as shown in Fig. 8.

3.2.3.3. Activation function. The activation function plays a significant role in introducing nonlinearity to the ML network. In general, the sigmoid or tanh function are the commonly utilized activation functions in Artificial Neural Network. However, this type of highly-nonlinear function puts the limit on the output, resulting in high computational cost. Therefore, the kind of activation is not favorable for CNN model which has a high requirement on computational capacities. To tackle these issues, the ReLU function without the limitation on output is utilized after every single convolutional layer.

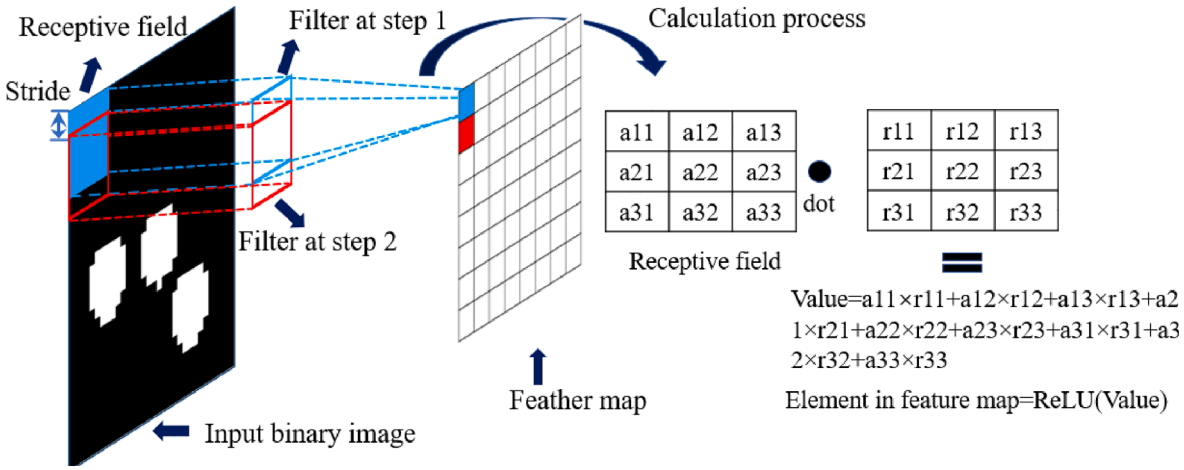

Fig. 9. Description of the convolution operation.

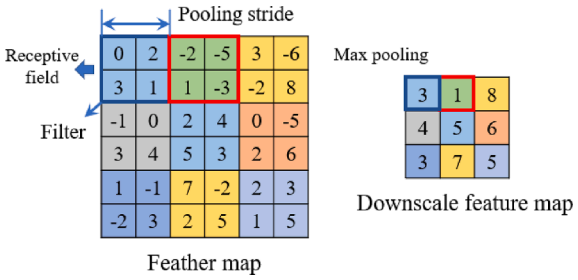

Fig. 10. Example for max-pooling layer.

4. Results and discussion

4.1. Crack pattern prediction

4.1.1. Model performance

In the lattice model, the crack pattern is a step-dependent descriptor of fracture behaviour, in which the number of broken elements depends entirely on the analysis step. As a data-driven method, the performance of CNN model for crack prediction is also highly influenced by the given crack patterns. Here, under the uniaxial tensile loading, a growing number of lattice elements are removed from the system to represent cracks. These broken elements eventually separate the numerical model into two parts, as shown in

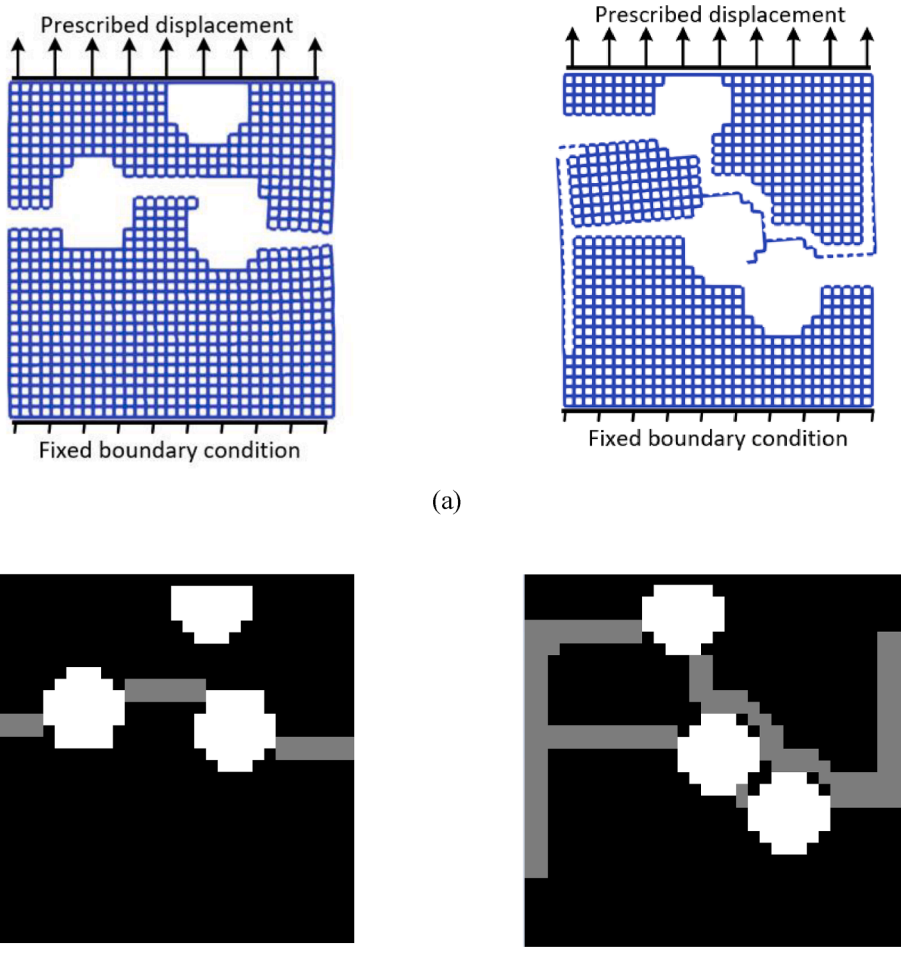

Fig. 11. Crack pattern for given microstructures (a) crack pattern in lattice model (b) crack pattern in digital image (gray: crack).

Fig. 11. It can be seen from the Fig. 11 the distribution of air voids within two microstructures significantly influences the crack patterns. In the first microstructure, a horizontal crack appears along with two pores at the mid-height, which is the weakest zone in the sample. In contrast, the second microstructure produces a complex crack pattern. The cracks initialize from the pore and propagate to the left and right boundary. This deformed structure results in a rotation on the zone around the middle pore. Another two cracks generate from the pore and develop to the neighbor pore and left boundary. The whole structure is then under the non-uniform deformation and eventually split into two parts. The detailed process of crack initialization and propagation can be found in Fig. 12. After structure fails, a complex crack pattern can be derived for this given microstructure.

For model validation, six randomly selected samples of predicted versus actual crack patterns are provided in Fig. 13. The first three microstructures process simple crack patterns and the U-Net CNN model predicts the same results. When comes to another three microstructures, the crack initialization and propagation are affected by external tensile loading and local rotation caused by the deformed structure. In the end, complex crack patterns can be found, like Fig. 11b. Based on the comparison results, it can be found that the U-net model achieves high prediction performance in testing data, with IoU being around 0.84. It demonstrates that U-Net model can correctly establish the relationship between the crack pattern and microstructure. This U-Net CNN model provides an alternative method for fracture analysis of composite materials with the input of the corresponding microstructure.

4.1.2. Feature map

This section discusses how the proposed U-net CNN model captures the features from the input binary image and gives the corresponding prediction on crack patterns under uniaxial tensile strength. Fig. 14 describes the feature maps derived from the convolutional layer in each Conv or Up-conv block. Since the convolution or deconvolution operation produces a series of feature maps whose size is equal to the channel size, the summation of these feature maps is computed along with the channel dimensionality to generate the results (as shown in Fig. 14). This model takes the binary image consisting of solid and air-void phases as input. The features in terms of the pore position are extracted and the derived feature map is close to the input microstructure. As it goes to the deeper Conv block, more details are extracted, therefore, the computed feature maps become abstract and uninterpretable. During the deconvolution process, the feature maps on small scale are utilized to extract information of each point to reproduce a larger image. In the last two feature maps, a clear feature map can be obtained, which correctly extracts the pore information and predicts the crack position. The pixels between or around the air-void zone have a deeper color after the convolution or deconvolution process, which suggests the crack initialization and propagation. This can provide some evidence that the U-net CNN model can extract the air-void information from the microstructure and output the correct crack pattern.

4.2. Stress-crack width curve prediction

4.2.1. Visualizing PCA

Considering the stress-crack width curve has a linear portion, the whole curve can be presented using a dimensional vector less than 101. To better understand the role of PCA in efficiently capturing the information stored in the stress-crack width curve, Fig. 15 (a) describes the relationship between the number of exponent principal components (r) and cumulative explained variance (CEV). Fig. 15 (b) lists the explained variance for the first 24 principal components. It can be illustrated that the first principal component has a cumulative explained variance around 0.4 and the first 24 principal components enable to represent the whole stress-crack width curve with cumulative explained variance higher than 99%. Through PCA, the lower-dimensional dataset with negligible loss of information about the stress-crack width curve can be derived, which ensures higher efficiency of model training. Three randomly chosen examples are given to demonstrate the difference between original and PCA inversed results (see Fig. 16).

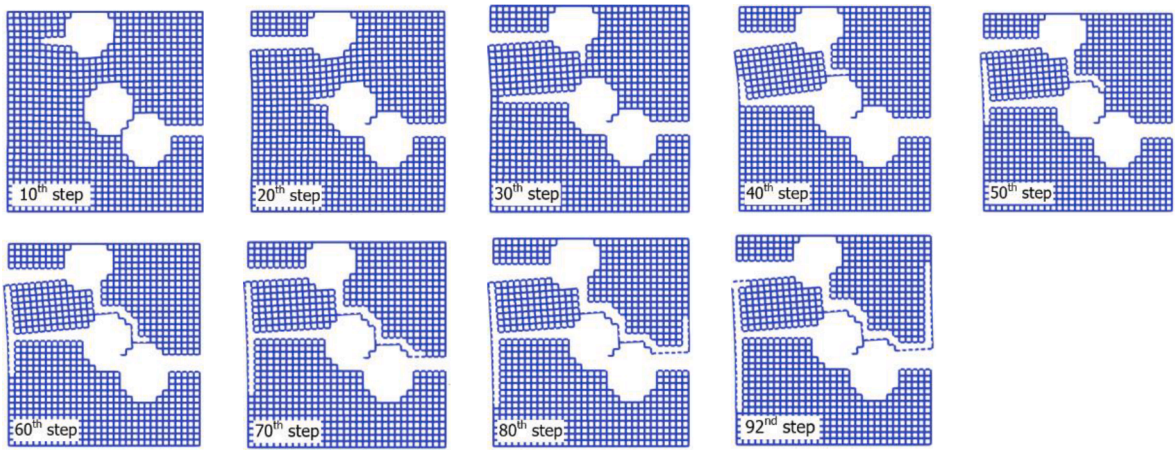

Fig. 12. Crack initialization and propagation under the uniaxial loading (white: crack element).

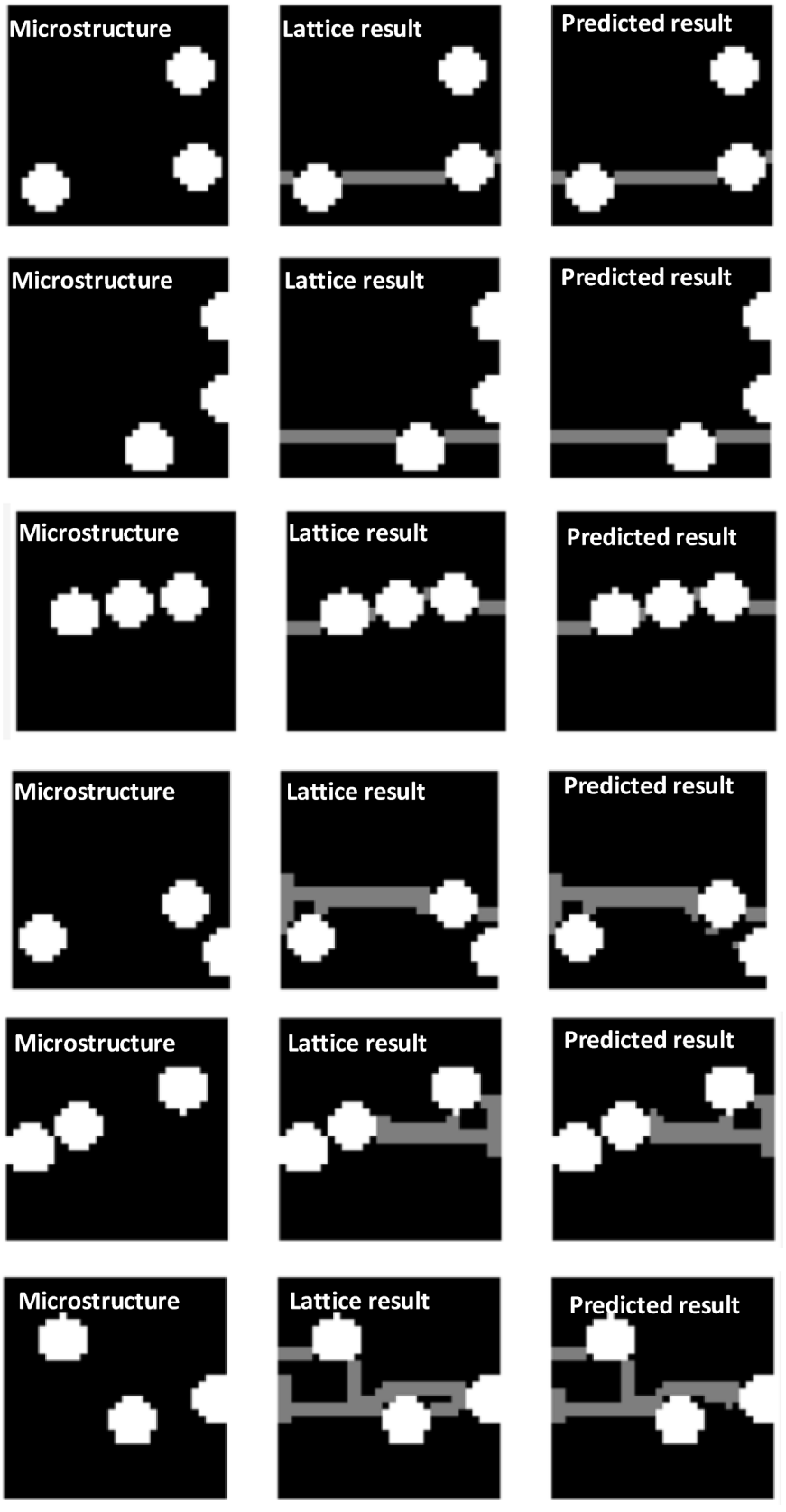

(caption on next page)

Fig. 13. Six random selected samples from test dataset for model evaluation (Gray: crack; white: pore; black: solid-matrix).

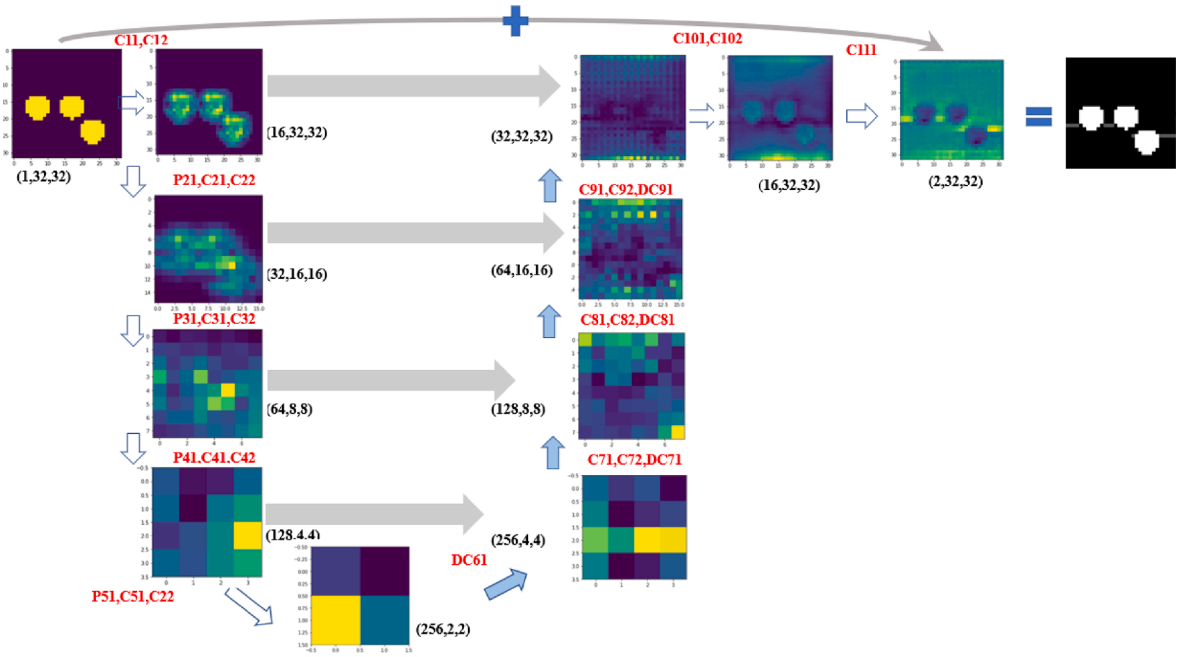

Fig. 14. Feature maps extracted from U-Net for crack pattern prediction.

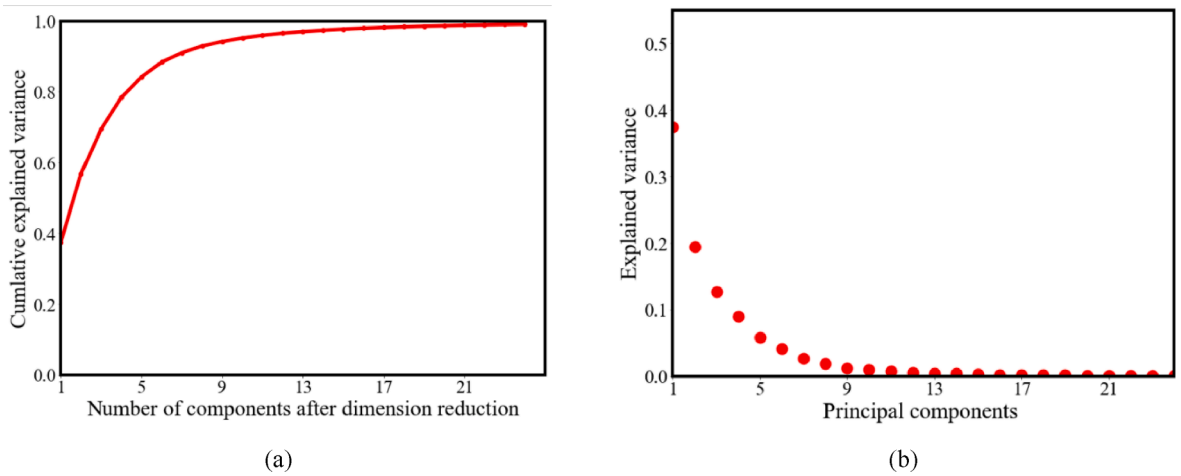

Fig. 15. (a) The relationship between the number of components after dimension reduction and cumulative explained variance (b) The explained variance for the first 20 principal components.

4.2.2. Model performance

In Fig. 17, six test samples that contain the stress-crack width curves are randomly selected to compare the prediction results from the CNN model and the lattice numerical analyses. The model performance during the training process is described in Fig. 18. The predicted results and model performance demonstrate that the proposed CNN model can accurately capture and learn the complex behaviour from the microstructures and establish the relationship between the digital images and stress-crack width curves. Besides, this new proposed model is more suitable for material properties prediction such as elastic modulus and strength since the predicted result becomes a scalar.

4.2.3. Feature map

This section explains how the proposed CNN model captures the features from the input binary image and forms the corresponding

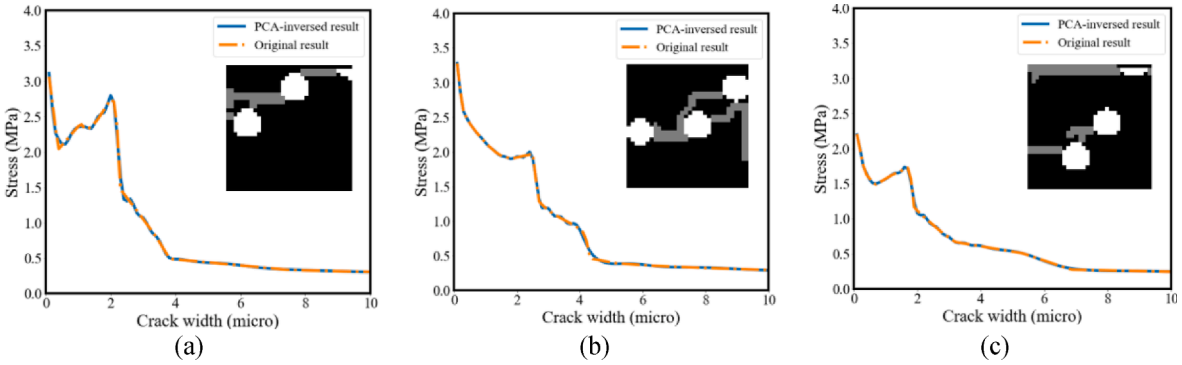

Fig. 16. A randomly chosen set of 3 predicted stress-crack width curves compared to the original and PCA inversed results.

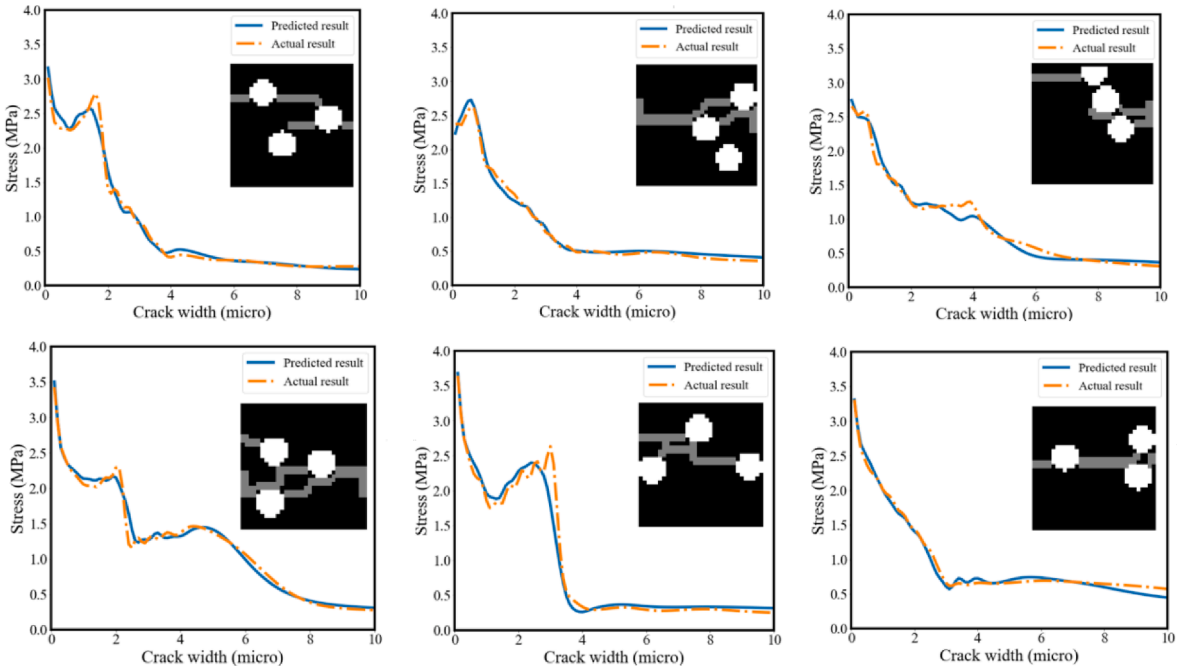

Fig. 17. A randomly chosen set of 6 predicted stress-crack width curves compared to the actual results from lattice model.

feature map for the next layer. As discussed in Section 3.2.3.1, through the step-by-step sliding process, the local feature of the microstructure can be extracted by the kernel to compute a series of feature maps, which is passed to the subsequent layer after ReLU activation and max-pooling operation. These extracted feature maps therefore emphasize the different importance of the local features. Fig. 19 describes the feature maps obtained from each convolutional layer in each Conv block. It should be noted that the convolution process produces a stack of feature maps. Here, the results in Fig. 19 are the summation of these feature maps along their channel. At the first Conv block, the features about the pore position are extracted and the derived feature map is similar to the input microstructure. The 2nd Conv block captures the interlayer between the air-void and solid matrix and compressed the derived feature maps into a smaller scale. As it goes to the deeper Conv block, more details are extracted therefore the computed feature maps become abstract and uninterpretable. For this given microstructure, the zone surrounded by air-void is the weak area, which significantly influences the stress-crack width curve. The 3rd Conv block shows that this zone is highlighted by the feature map. This can explain why the CNN model can analyze the microstructure and predict the stress-crack width curve.

4.3. Discussion on model generalization

Through the training process, these two proposed CNN models achieve approximation functions that can fit the training and test sets with acceptable errors. The results show the high performance in the predictions of stress-crack width curves and crack patterns based on the input microstructure. However, this is one of the ideal scenarios during the CNN training process. Besides, a good

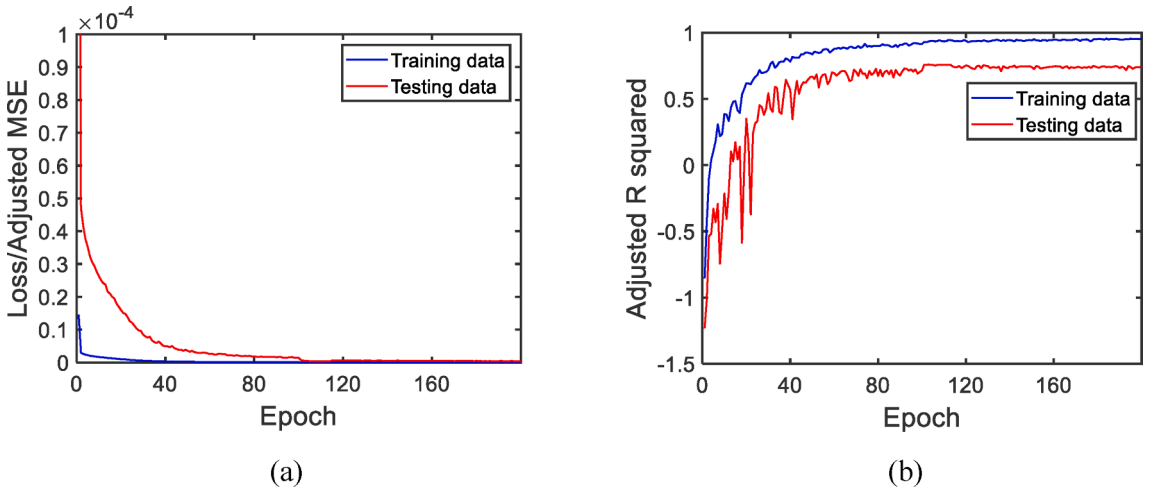

Fig. 18. Model performance during the training process (a) adjusted loss (b) adjusted R squared.

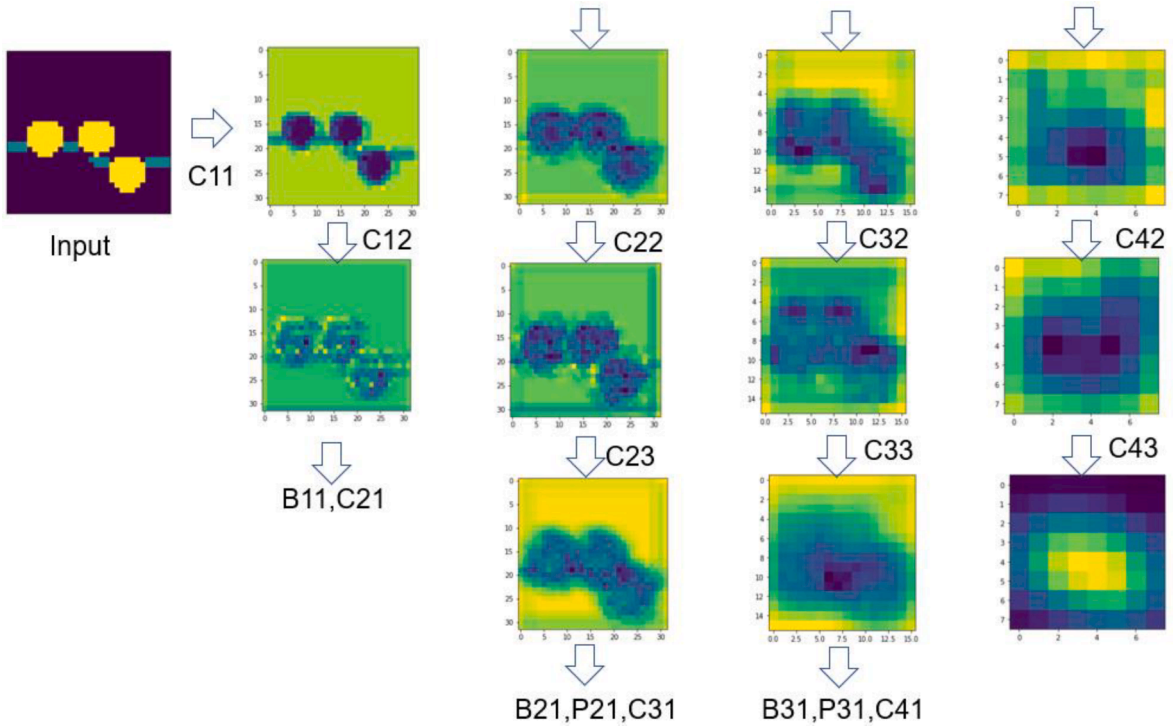

Fig. 19. Feature maps extracted from CNN for stress-crack width curve prediction.

generalization is what we aim to achieve. Model generalization refers to the model performance of the trained network for the new, previously unseen data. In general, the generalization gap can be found in machine learning algorithms, i.e., a difference between a model's performance on the training data and its performance on an unseen dataset that consists of different kinds of samples. In this study, the model generalization will be discussed in the following procedures.

First, these two pre-trained CNN models will be evaluated using the unseen datasets from group 2, which contains the samples with different pore information (i.e., pore number and pore size). Based on these results, transfer learning with adaptive fine-tuning is utilized to check the model efficiency on different microstructures. Transfer learning is a machine learning technique in which a model created for one task is used as the foundation for another task. Adaptive fine-tuning is the method of adjusting a portion of a model's parameters extremely precisely to fit specific data [48]. Here, 5 other kinds of microstructures are utilized from model performance evaluation, and the typical microstructures for each kind of set are given in the Fig. 20.

The pre-trained models are then utilized for model generalization discussion by means of the above 5 kinds of microstructures, in

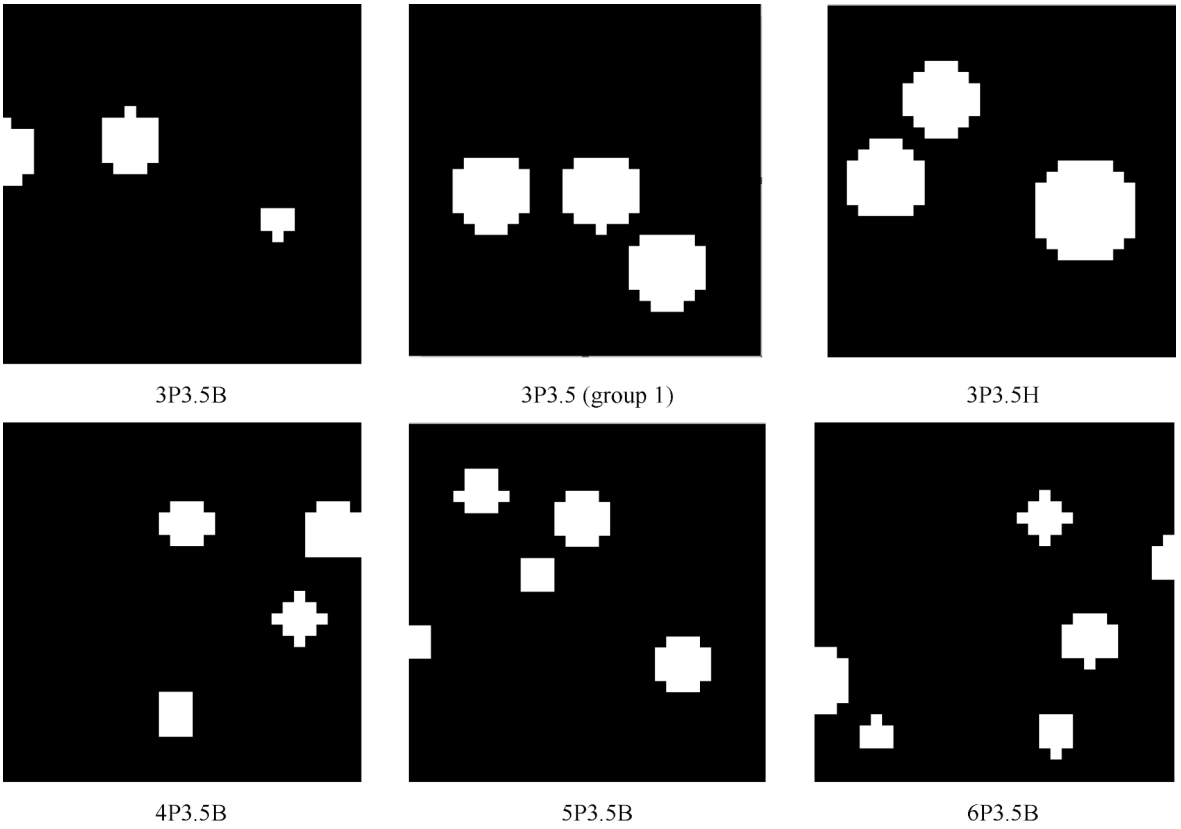

Fig. 20. Digital structures from dataset 2 (3P3.5H represent the microstructure including three air-voids with the diameter above 3.5; 6P3.5B refers to the microstructure containing six pores with the diameter below 3.5).

which 5,000 samples of each type are randomly chosen for model testing. The adjusted R^2 and IoU which describe the model performance in terms of crack pattern and the stress-crack width curve are shown in Fig. 21.

Regarding the crack prediction, it can be illustrated from Fig. 21 (a) that the U-Net CNN model also performed well on the unseen microstructures, which include more complex pore information about number and size. All computed IoU values are higher than 0.64. The air-void location is dominant when the fracture initiates and propagates. The high IoU values suggested the trained U-Net model can efficiently capture the characteristic of air-void position. This is because the convolutional process extracts the pore location feature during the down-sampling process, and the concatenation process transmits spatial correlation during the up-sampling step. As a result, the important information for pore localization is preserved, and a satisfactory result about model generalization can be achieved utilizing the U-net model for crack pattern prediction. Compared to the IoU from the dataset named 3P3.5, these IoU values are a little bit lower. This is because of the insufficiency or deficiency of the new microstructures on the training dataset. To further check whether this proposed U-net model can better clarify the relationship between the microstructure and fracture performance of binary composites with quite different pore information, the dataset named 5P3.5B is employed for model training. The pre-trained weights from group 1 are taken as initial values and 35,000 samples are adopted to update weights by fine-tuning with a learning rate of 0.0001. The remaining 5,000 cases are then adopted for model validation and the computed IoU is increased from 0.655 to 0.71, with 8.4 % accuracy increase, as shown in Fig. 21 (a). Three typical samples randomly picked up from the validation dataset are given in Fig. 22 to show model performance. Although some minor difference exists between the predicted and the actual results, the U-Net model with updated trainable parameters correctly captures the feature of input digital structure and produces a similar crack pattern with the ground result. Increasing the number of training samples can achieve a better model performance.

It can be observed from Fig. 21 (b) that the CNN model for stress-crack width curve prediction generates poor performance at the unseen test dataset, which can be easily explained by the lack of unseen cases in the training dataset. Unlike fracture pattern prediction, the prediction of stress-crack width curve is controlled by two factors: porosity and pore location. The well-trained CNN model can extract features including pore location, as explained before. However, for samples with varied porosity, the trained weights in this model may be less accurate. Consequently, model generalization produces poor performance. To improve model performance, transfer learning with fine-tuning is utilized, which means that the pre-trained parameters are adopted as initial weight and continue to be trained. In this study, the pre-trained weights from the last two convolutional blocks are frozen together with the last linear layer. The microstructure that contains five pores with a diameter below 3.5 mm is taken as an example for model generalization discussion, in which a dataset including 115,000 samples with a train/test split ratio of 95:5 is adopted. To verify the pre-trained weights on the new

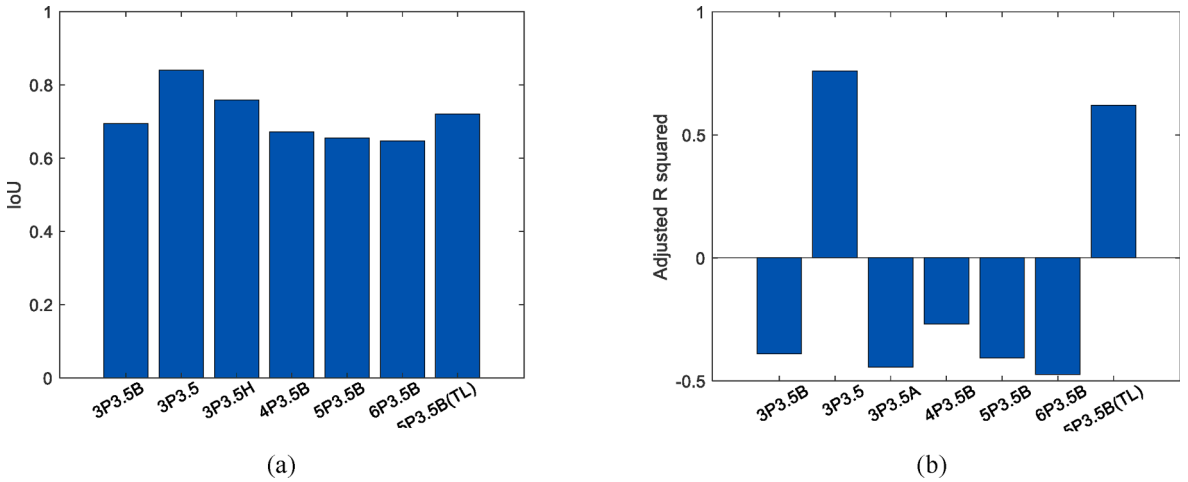

Fig. 21. Model performance with unseen microstructures (a) IoU for crack prediction (TL: transfer learning) (b) adjusted R2 for stress-crack width curve.

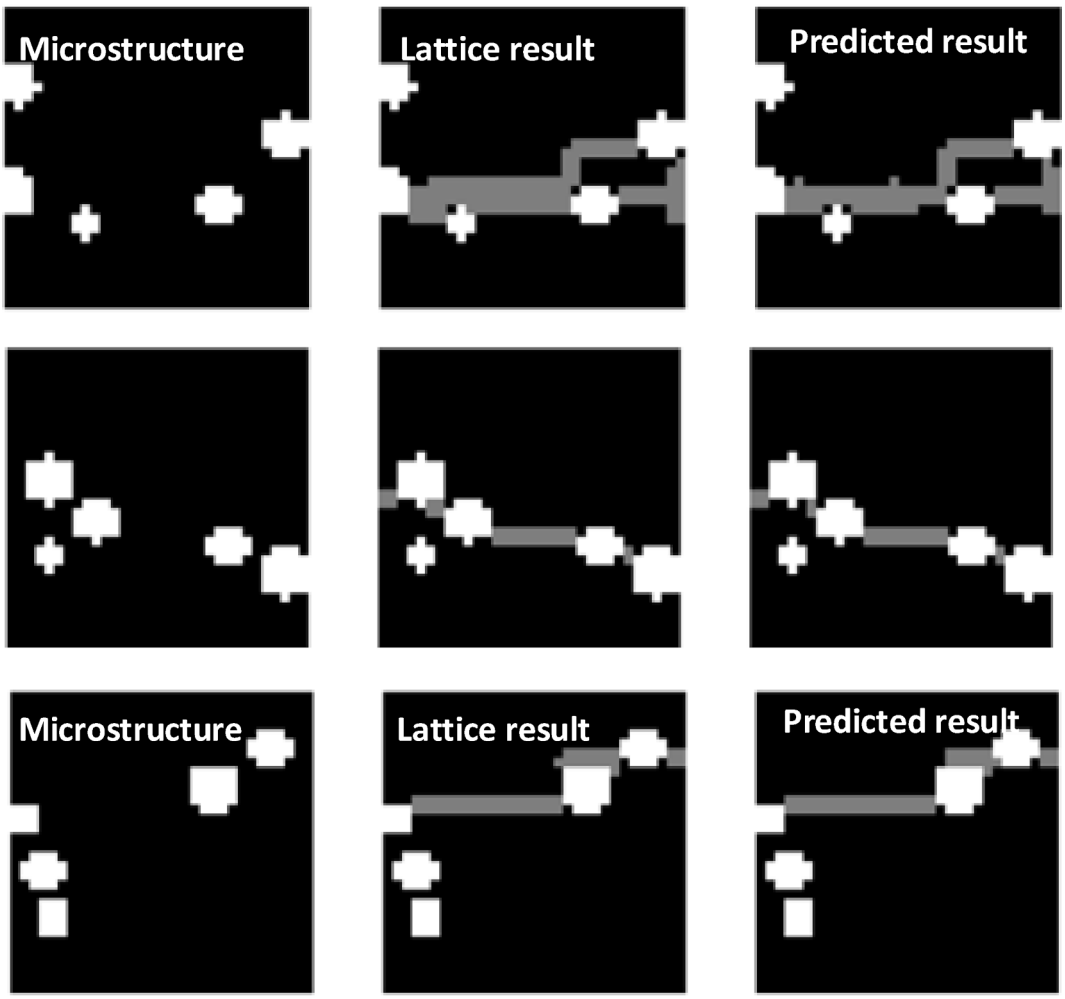

Fig. 22. A randomly selected set of three predicted crack patterns compared to simulated crack pattern.

dataset, the equivalent number of datasets are also trained using the model with the same hyperparameter configuration without the pre-trainable weight from group 1. The training history can be found in Fig. 23. It can be illustrated that the model with transfer learning not only avoids the obvious overfitting issue but also produces a higher adjusted R^2. It suggests the pre-trained parameters based on group 1 provide the correct initial weight on the trainable parameter for stress-crack width prediction. Three randomly chosen cases are provided to demonstrate model performance, as shown in Fig. 24.

5. Model application

The previous analyses show the model application on fracture analysis of air-void systems with relatively simple pore information. One of the goals of this study is to use the proposed CNN model to do some fracture analyses with 3D printed materials. The input image representing 3D printed concrete can be created through two methods. The first one is to crop the data to the same proportions as the input image. The second one is to reshape an XCT cropped image that is rather large. Data loss is inevitable when resizing the clipped XCT picture, especially for the disappearance of tiny pores. But the rather large air-voids remain after image reshaping, which have a greater impact on the fracture pattern. Besides, compared to the first method, the input picture obtained using the second approach still contains more complicated pore information. Therefore, the second approach is used to collect input images. To create a database that describes the air-void distribution of 3D printed materials, 53,573 slices of 160 * 160 pixels 2D microstructure are cropped from XCT images of 3D printed samples. These images are then resized to 32 by 32 pixels digital structures, which equals the input shape in U-net model. A schematic diagram is given in Fig. 25 to describe the generation of microstructure.

The pre-trained U-net model is adopted for crack prediction, in which 50,000 specimens are utilized for model training and the rest 3,575 are employed for model validation. The batch size for all sets is set to 64 and the Adam optimizer with the learning rate of 0.0005 is employed for fine-tuning by means of transfer learning. For model validation, three randomly selected samples of predicted versus actual crack patterns are provided in Fig. 26. It can be found that the U-net model predicts the similar crack pattern with lattice numerical analysis, with the IoU value around 0.73. It demonstrates that the proposed U-net model for crack pattern prediction is not limited to the microstructure with simply air-void information. It is also valid to the microstructures cropped from XCT and the predicted crack information is close to the ground truth.

Since domain shift is a significant problem for ML, the different model performance may be observed for various air-void structures. Images from XCT indicate a superior result compared to model performance on samples with five pores information. This is because more data is utilized for fine-tuning. Model performance on samples with three pore information outperforms that of the XCT image. This is due to the fact that the XCT images display more complicated air-void features, such as pore size, distribution, and position. Meanwhile, more data is used for model training on the sample with three pores, implying in a higher IoU.

6. Future work

In this research, the predictions that are obtained are found after training of datasets obtained from simulations with the lattice fracture model. The crack pattern and stress-crack width curve can be accurately predicted with the microstructure as input. The results of this model are compared with experimental data in other research projects and always a very good match is obtained. For these microstructures with air voids the simulations with the lattice model will be compared in future research to experimental data to increase the confidence level.

In the cases investigated the sample is loaded in uniaxial tension, which means a uni-directional stress field is created. In future research it will be investigated if predictions of with complicated stress field also result in correct crack patterns and stress-crack width

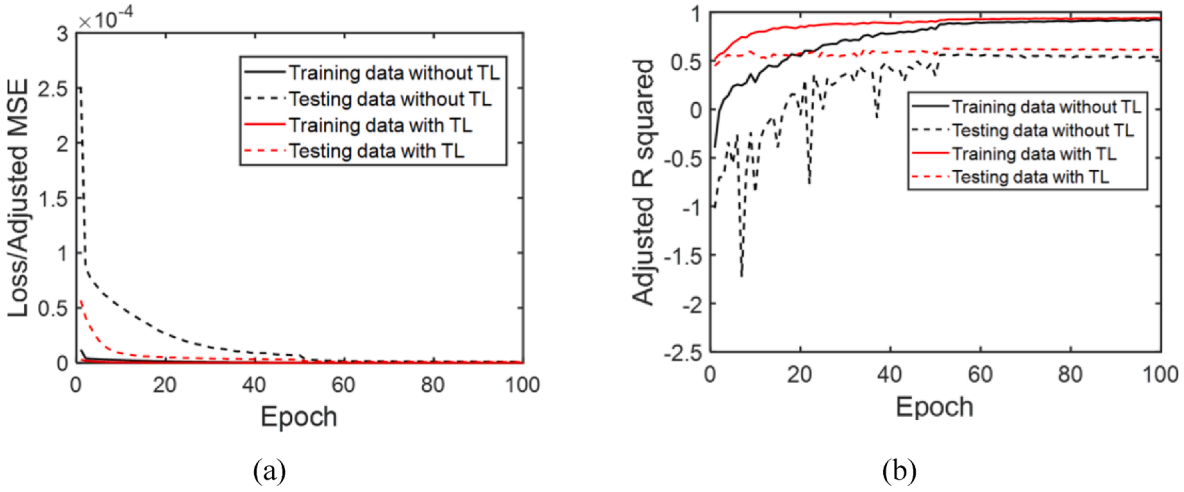

Fig. 23. Model performance (a) Adjusted MSE during the training process (b) adjusted R^2 during the training process (TL: transfer learning).

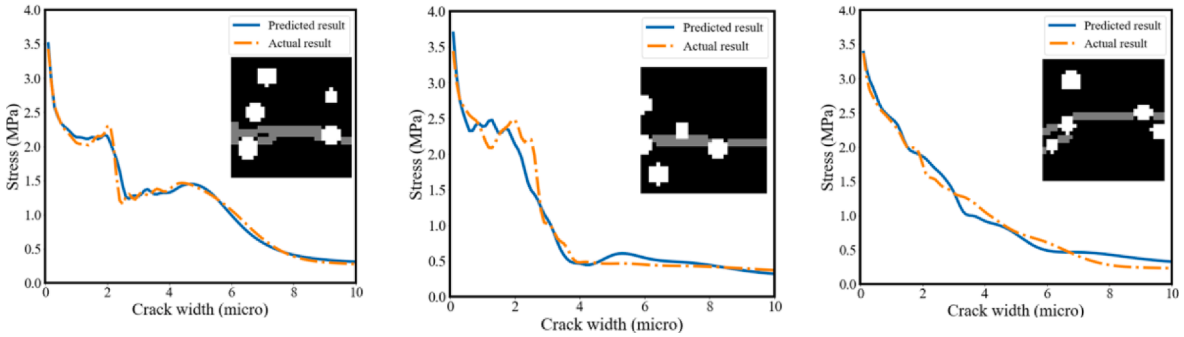

Fig. 24. A randomly chosen set of three predicted stress-crack width curves after transfer learning compared to the actual results from the lattice model.

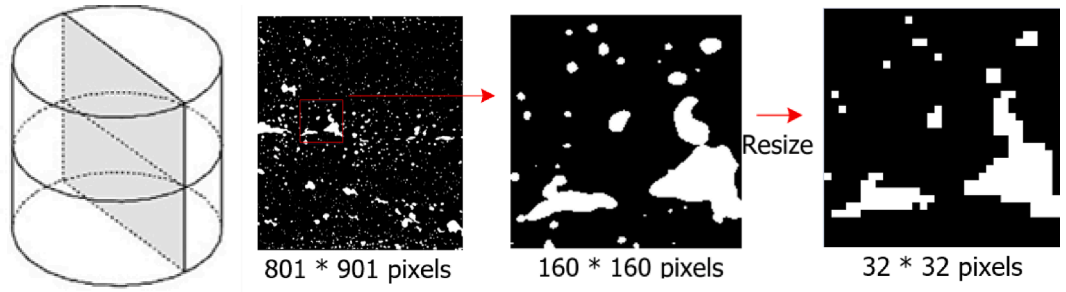

Fig. 25. Generation of microstructure from XCT images.

results.

In future we will also study more complicated microstructures that not only contain air voids in a matrix, but more heterogeneous microstructures with particles with varying properties.

Besides, further work includes combing the proposed CNN model for stress-crack width curve prediction and lattice fracture model to do multi-scale fracture modelling of 3D printed materials. In addition, the lattice model adopts the crack pattern as a step-dependent descriptor of fracture behaviour. Thus, the time-dependent crack formulation can be derived based on the analysis step. We plan to explore the crack initialization and propagation of composite materials by means of recurrent neural network.

7. Conclusion

In this study, according to the air-void distribution in 3DCP, the binary images with various air-void information are created for CNN datasets. Subjected to the uniaxial tensile loading, their corresponding stress-crack width curves and crack patterns can be derived using the lattice fracture model. Then two CNN models are proposed to predict the stress-crack width curves and crack formulations given the air-void structures as input. During the training process, the customized loss function, *R*-squared and IoU are provided to show the model performance. A further investigation for model generalization is conducted using transfer learning with adaptive fine-tuning. Through this research model, the following conclusions can be reached:

(1) The U-Net CNN model was used to solve the issues related to semantic segmentation; it also shows the feasibility for crack prediction of air-void structure. These two CNN models can be considered as alternative methods to decrease the computational cost for mechanical and fracture analyses of binary composites.
(2) The self-developed U-Net model was trained based on the microstructure including three pores with a diameter of 3.5. This trained model can be directly utilized for crack prediction of microstructures with different pore information. Introducing more unseen datasets to the training process through transfer learning can achieve a higher model performance.
(3) The CNN model can achieve high accuracy for stress-crack width curve prediction towards specific microstructures. Based on the transfer learning with fine-tuning, it is easy to clarify the relation between mechanical behaviour with other kinds of microstructures. These pre-trained weights can remedy the issue of data deficiency and avoid overfitting.
(4) The proposed U-Net model for crack pattern prediction is not limited to the microstructure with simply air-void information. It is also valid to the microstructures cropped from XCT and the predicted crack information is close to the ground truth.

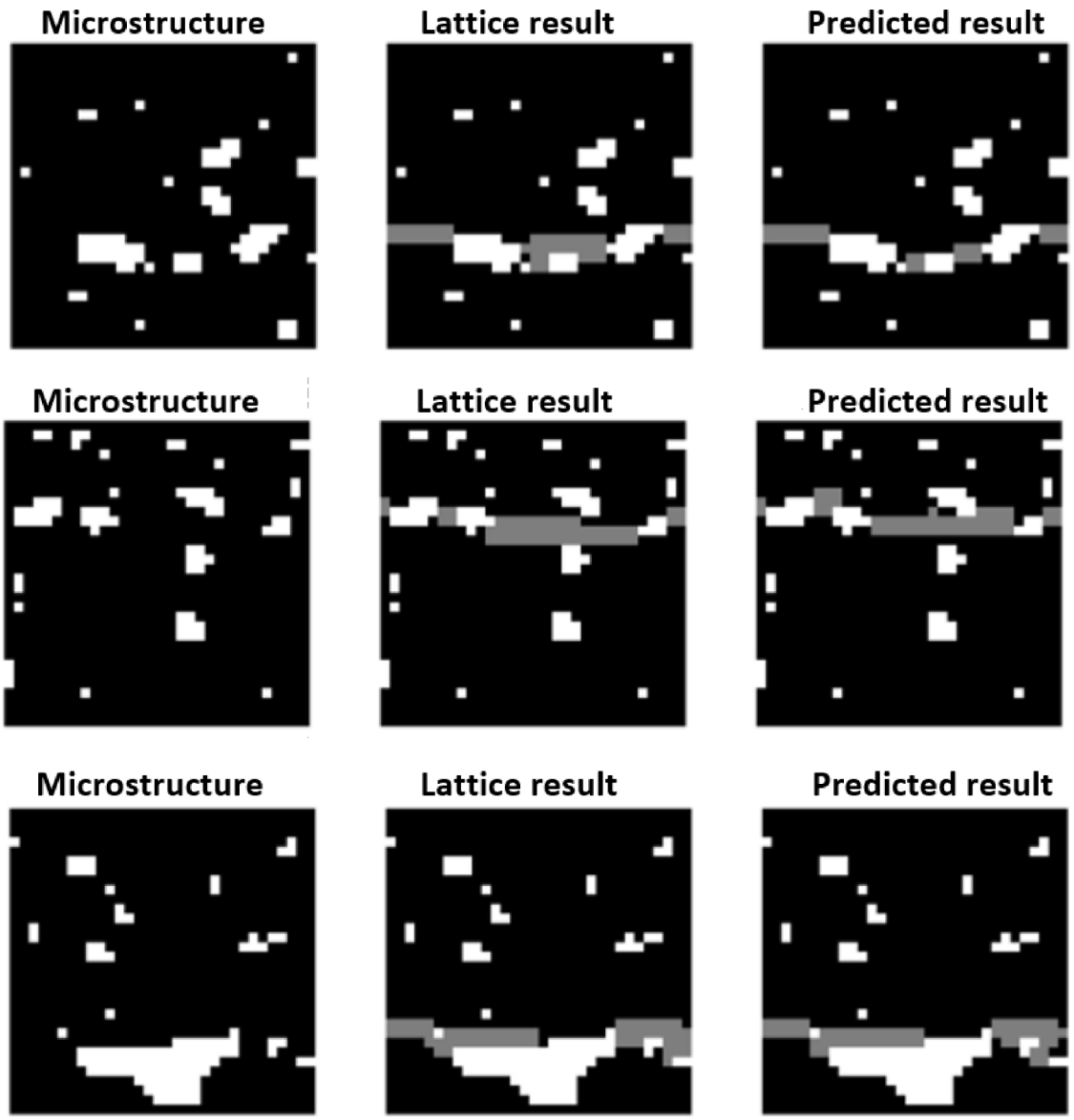

Fig. 26. Three random selected samples from test dataset for model evaluation (Gray: crack; white: pore; black: solid-matrix).

CRediT authorship contribution statement

Ze Chang: Conceptualization, Methodology, Data curation, Writing – original draft, Software. **Zhi Wan:** Conceptualization, Methodology, Data curation, Writing – review & editing. **Yading Xu:** Conceptualization, Writing – review & editing. **Erik Schlangen:** Supervision, Conceptualization, Writing – review & editing. **Branko Šavija:** Supervision, Conceptualization, Methodology, Data curation, Writing – review & editing.

Declaration of Competing Interest

The authors declare that they have no known competing financial interests or personal relationships that could have appeared to influence the work reported in this paper.

Acknowledgements

Ze Chang and Zhi Wan would like to acknowledge the funding supported by China Scholarship Council under Grant No. 201806060129 and 201906220205, respectively. Yading Xu and Branko Šavija acknowledge the financial support of the European

Research Council (ERC) within the framework of the ERC Starting Grant Project "Auxetic Cementitious Composites by 3D printing (ACC-3D)", Grant Agreement Number 101041342.

References

[1] Perrot A, Pierre A, Nerella VN, Wolfs RJM, Keita E, Nair SAO, et al. Mechtcherine, From analytical methods to numerical simulations: A process engineering toolbox for 3D concrete printing. Cem Concr Compos 2021;122:104164. https://doi.org/10.1016/j.cemconcomp.2021.104164.
[2] Buswell RA, da Silva WL, Bos FP, Schipper H, Lowke D, Hack N, et al. A process classification framework for defining and describing Digital Fabrication with Concrete. Cem Concr Res 2020;134:106068.
[3] Nerella VN, Hempel S, Mechtcherine V. Effects of layer-interface properties on mechanical performance of concrete elements produced by extrusion-based 3D-printing. Constr Build Mater 2019;205:586–601.
[4] Wolfs RJM, Bos FP, Salet TAM. Hardened properties of 3D printed concrete: The influence of process parameters on interlayer adhesion. Cem Concr Res 2019;119:132–40.
[5] Chen Y, Chang Z, He S, Çopuroğlu O, Šavija B, Schlangen E. Effect of curing conditions during a long-time gap on the interlayer bonding of 3D printed cementitious materials. Constr Build Mater 2022;332:127394.
[6] Panda B, Mohamed N, Ahamed N, Paul SC, Bhagath Singh G, Tan MJ, et al. The effect of material fresh properties and process parameters on buildability and interlayer adhesion of 3D printed concrete. Materials 2019;12(13):2149.
[7] Chen Y, Jansen K, Zhang H, Rodriguez CR, Gan Y, Çopuroğlu O, et al. Effect of printing parameters on interlayer bond strength of 3D printed limestone-calcined clay-based cementitious materials: An experimental and numerical study. Constr Build Mater 2020;262:120094.
[8] Zareiyan B, Khoshnevis B. Interlayer adhesion and strength of structures in Contour Crafting - Effects of aggregate size, extrusion rate, and layer thickness. Autom Constr 2017;81:112–21.
[9] Chen Y, Çopuroğlu O, Rodriguez CR, de Mendonca Filho FF, Schlangen E. Characterization of air-void systems in 3D printed cementitious materials using optical image scanning and X-ray computed tomography. Mater Charact 2021;173:110948.
[10] Keita E, Bessaies-Bey H, Zuo W, Belin P, Roussel N. Weak bond strength between successive layers in extrusion-based additive manufacturing: measurement and physical origin. Cem Concr Res 2019;123:105787. https://doi.org/10.1016/j.cemconres.2019.105787.
[11] Kruger J, du Plessis A, van Zijl G. An investigation into the porosity of extrusion-based 3D printed concrete. Addit Manuf 2021;37:101740.
[12] Feng P, Meng X, Chen J-F, Ye L. Mechanical properties of structures 3D printed with cementitious powders. Constr Build Mater 2015;93:486–97.
[13] Bolander JE, Shiraishi T, Isogawa Y. An adaptive procedure for fracture simulation in extensive lattice networks. Engng Fract Mech 1996;54(3):325–34.
[14] Zhang H, Šavija B, Schlangen E. Combined experimental and numerical study on micro-cube indentation splitting test of cement paste. Engng Fract Mech 2018;199:773–86.
[15] Bolander JE, Saito S. Fracture analyses using spring networks with random geometry. Engng Fract Mech 1998;61(5-6):569–91.
[16] Schlangen E, Garboczi EJ. Fracture simulations of concrete using lattice models: computational aspects. Engng Fract Mech 1997;57(2-3):319–32.
[17] Chang Z, Zhang H, Schlangen E, Šavija B. Lattice Fracture Model for Concrete Fracture Revisited: Calibration and Validation. Applied Sciences 2020;10(14):4822.
[18] Prasad BKR, Eskandari H, Reddy BVV. Prediction of compressive strength of SCC and HPC with high volume fly ash using ANN. Constr Build Mater 2009;23(1):117–28.
[19] Park JY, Yoon YG, Oh TK. Prediction of concrete strength with P-, S-, R-wave velocities by support vector machine (SVM) and artificial neural network (ANN). Appl Sci 2019;9(19):4053.
[20] Yang C, Kim Y, Ryu S, Gu GX. Prediction of composite microstructure stress-strain curves using convolutional neural networks. Mater Des 2020;189:108509.
[21] Lee J, Oh SJ, An SH, Kim W-D, Kim S-H. Machine learning-based design strategy for 3D printable bioink: elastic modulus and yield stress determine printability. Biofabrication 2020;12(3):035018.
[22] Han T, Siddique A, Khayat K, Huang J, Kumar A. An ensemble machine learning approach for prediction and optimization of modulus of elasticity of recycled aggregate concrete. Constr Build Mater 2020;244:118271.
[23] Kruger J, Cho S, Zeranka S, Viljoen C, van Zijl G. 3D concrete printer parameter optimisation for high rate digital construction avoiding plastic collapse. Compos B Engng 2019;183:107660.
[24] Liu R, Kumar A, Chen Z, Agrawal A, Sundararaghavan V, Choudhary A. A predictive machine learning approach for microstructure optimization and materials design. Sci Rep 2015;5(1):1–12.
[25] Ziolkowski P, Niedostatkiewicz M. Machine learning techniques in concrete mix design. Materials 2019;12(8):1256.
[26] Gujar R, Vakharia V. Prediction and validation of alternative fillers used in micro surfacing mix-design using machine learning techniques. Constr Build Mater 2019;207:519–27.
[27] Ziolkowski P, Niedostatkiewicz M, Kang S-B. Model-Based Adaptive Machine Learning Approach in Concrete Mix Design. Materials 2021;14(7):1661.
[28] Cheng L, Xin H, Groves RM, Veljkovic M. Acoustic emission source location using Lamb wave propagation simulation and artificial neural network for I-shaped steel girder. Constr Build Mater 2021;273:121706.
[29] Xin H, Cheng L, Diender R, Veljkovic M. Fracture acoustic emission signals identification of stay cables in bridge engineering application using deep transfer learning and wavelet analysis. Adv Bridge Eng 2020;1(1):1–16.
[30] Dung CV, Anh LD. Autonomous concrete crack detection using deep fully convolutional neural network. Autom Constr 2019;99:52–8.
[31] Cha Y-J, Choi W, Büyüköztürk O. Deep learning-based crack damage detection using convolutional neural networks. Comput-Aided Civ Infrastruct Engng 2017;32(5):361–78.
[32] Na J, Kim G, Kang S-H, Kim S-J, Lee S. Deep learning-based discriminative refocusing of scanning electron microscopy images for materials science. Acta Mater 2021;214:116987.
[33] Davtalab O, Kazemian A, Yuan X, Khoshnevis B. Automated inspection in robotic additive manufacturing using deep learning for layer deformation detection. J Intell Manuf 2022;33(3):771–84.
[34] Liang M, Gan Y, Chang Z, Wan Z, Schlangen E, Šavija B. Microstructure-informed deep convolutional neural network for predicting short-term creep modulus of cement paste. Cem Concr Res 2022;152:106681.
[35] Kim D-W, Lim JH, Lee S. Prediction and validation of the transverse mechanical behavior of unidirectional composites considering interfacial debonding through convolutional neural networks. Compos B Engng 2021;225:109314.
[36] Hsu Y-C, Yu C-H, Buehler MJ. Using deep learning to predict fracture patterns in crystalline solids. Matter 2020;3(1):197–211.
[37] Elapolu MS, Shishir MIR, Tabarraei A. A novel approach for studying crack propagation in polycrystalline graphene using machine learning algorithms. Comput Mater Sci 2022;201:110878.
[38] Schwarzer M, Rogan B, Ruan Y, Song Z, Lee DY, Percus AG, et al. Learning to fail: Predicting fracture evolution in brittle material models using recurrent graph convolutional neural networks. Comput Mater Sci 2019;162:322–32.
[39] Pierson K, Rahman A, Spear AD. Predicting microstructure-sensitive fatigue-crack path in 3d using a machine learning framework. Jom 2019;71(8):2680–94.
[40] Wang Y, Oyen D, Guo W(, Mehta A, Scott CB, Panda N, et al. StressNet-Deep learning to predict stress with fracture propagation in brittle materials. npj Mater Degrad 2021;5(1). https://doi.org/10.1038/s41529-021-00151-y.
[41] Wei H, Yao H, Pang Y, Liu Y. Fracture Pattern Prediction with Random Microstructure using a Physics-Informed Deep Neural Networks. Engng Fract Mech 2022;268:108497.
[42] Jiang N, Zhang H, Chang Z, Schlangen E, Ge Z, Šavija B. Discrete lattice fracture modelling of hydrated cement paste under uniaxial compression at micro-scale. Constr Build Mater 2020;263:120153.

[43] Zhang H, Xu Y, Gan Y, Schlangen E, Šavija B. Experimentally validated meso-scale fracture modelling of mortar using output from micromechanical models. Cem Concr Compos 2020;110:103567.
[44] Šavija B, Luković M, Pacheco J, Schlangen E. Cracking of the concrete cover due to reinforcement corrosion: A two-dimensional lattice model study. Constr Build Mater 2013;44:626–38.
[45] Chang Ze, Xu Y, Chen Yu, Gan Y, Schlangen E, Šavija B. A discrete lattice model for assessment of buildability performance of 3D-printed concrete. Computer-Aid Civ Infrastruct Eng 2021;36(5):638–55.
[46] Berman M, Triki AR, Blaschko MB. The lovász-softmax loss: A tractable surrogate for the optimization of the intersection-over-union measure in neural networks. In: Proceedings of the IEEE conference on computer vision and pattern recognition; 2018. p. 4413–21.
[47] Ronneberger O, Fischer P, Brox T. U-net: Convolutional networks for biomedical image segmentation, International Conference on Medical image computing and computer-assisted intervention. Springer; 2015. p. 234–41. https://doi.org/10.1007/978-3-319-24574-4_28.
[48] Guo Y, Shi H, Kumar A, Grauman K, Rosing T, Feris R. Spottune: transfer learning through adaptive fine-tuning. In: Proceedings of the IEEE/CVF conference on computer vision and pattern recognition; 2019. p. 4805–14.